Cryogenically Cooled Yb:YAG Ceramic Amplifier Module for High Power Lasers

by

Muhammad Raj Masud

A thesis submitted in partial fulfillment of the requirements for the degree of

Master of Science

in

Photonics and Plasmas

Department of Electrical and Computer Engineering
University of Alberta

Abstract

A new class of direct diode pumped ceramic disk lasers are emerging as attractive candidates for efficient high power amplifiers in industrial and scientific applications. This thesis discusses the development and characterization of a high gain laser module based on Yb:YAG ceramic laser media which can be scaled to high power and high energy output for such applications. Measurements of gain and extracted energy have been carried out at room temperature as well as at cryogenic temperature. The results are then compared to rate equation modeling of the pulse amplification as a function of temperature and input pulse fluence. Temperature dependent cross-section values and the variation of lower level population according to Boltzmann distribution were considered in our calculations. The literature values of the cross-section and carrier lifetime that gave the best match with the experimental data are summarized in this work. The limitations in operating condition due to transverse/parasitic lasing were also explored and possible solutions were discussed. Based on the measurements and the simulations, a terawatt pulse system configuration is proposed.

Preface

A summary of this thesis has been published as M. R. Masud, H. Tiedje, I. Utkin, and R. Fedosejevs, "Cryogenically Cooled Yb:YAG Ceramic Amplifier Modules for High Power Lasers," Physics in Canada, vol. 71, issue 1, Masu 1- Masu3, 2015. I was responsible for experimental setup, data collection and analysis, simulation as well as manuscript editing. H. Tiedje has provided the initial training and also helped in building the amplifier setup, developed the main power supply of the diode pump, and provided constant support in every step of the project, and supported me with his advice and suggestions. I. Utkin has helped me by building the first version of the laser oscillator, provided the temperature sensors, and supported with his valuable advice and suggestions. R. Fedosejevs was the supervisory author and was involved with concept formation, experimental setup finalization, manuscript composition, and continuous advice and suggestions.

The room temperature measurements and initial cryogenic measurement data was presented as M.R. Masud, H.F. Tiedje, I. Utkin, T. Schoepp, Y. Yu and R. Fedosejevs, "Diode Pumped Yb:YAG Ceramic Laser Amplifier Modules for a TW Laser System," Annual Congress of the Canadian Association of Physicists, Sudbury, June 16-20, 2014. T. Schoepp and Y. Yu participated in discussions from time to time beside the major contributions of H. Tiedje, I. Utkin, and R. Fedosejevs.

After Allah, the Almighty

I dedicate this thesis to

My beloved wife, Rokshana Akter Himi

My cute little daughter, Suhaila Binte Masud

and

My wonderful parents, M. Ala Uddin and Ayesha Akter

Acknowledgements

I would like to express my deepest gratitude to my thesis supervisor, Dr. Robert Fedosejevs, for his constant support, invaluable advice, and constructive evaluation towards this thesis. He has not only supported my research work but also provided great emotional support to keep up my confidence in many difficult moments on the road to finish this thesis. I also appreciate him for providing me with the opportunity to work in the large facilities such as Lawrence Livermore National Laboratory in USA and Advanced Laser Light Source in Canada. He has been my role model in research who taught me to believe that everything happens for a reason and nature does not lie. Very importantly, he has always guided me to thrive both as an individual and as a team member.

I would also like to sincerely thank my M. Sc. exam committee, Dr. Tsui Ying and Dr. Jaeger for their valuable comments, questions, and recommendations.

My warmest thanks to my wonderful parents, M. Alauddin and Ayesha Akter for having their trust on me. They have been through a lot of hardships, but never allowed a drop of it to touch me. I could make this far in my life only because of their trust and support. They were thousands of miles away from me, but their love and inspiration were always with me.

I also express my loving thanks to my sweet little daughter, Suhaila. After a tiring day of work in the laboratory, her single smile was sufficient for me to forget everything.

I express my utmost appreciation to my wife, Himi who has been my strength and encouragement during the weakest moments of my graduate school and life. Her sacrifices and support could never be expressed in words. I could just say that without her support nothing would be possible. During my graduate life, I have been immersed into my research work, while she took care of everything else. I could not ask for more than what she has already done for me.

Table of Contents

List of Tables

List of Figures

Chapter 1 Introduction

1.1 Motivation

High energy ultrashort laser pulses are becoming the primary tool of many research areas ranging from materials processing [1] to amplification of ultrashort pulses to extremely high intensities for high energy particle acceleration [2], x-ray generation [3] and Fast Ignition Laser Fusion [4]. For applications requiring joule level pulses, concentrating all the energy in a picosecond or femtosecond pulse would make the pulse intensity large enough to easily damage the optics in the cavity. Therefore, the optical pulses should be amplified outside the cavity where these limitations can be overcome. Ultrashort optical pulses (femtosecond to picosecond) can be amplified to high energies by chirped pulse amplification (CPA) [4], where the pulse is stretched in time by a factor of 100 or 1000 times before amplification to avoid high intensity optical damage. Due to the minimum Fourier time-bandwidth product, short pulses naturally have a large bandwidth, which allows the use of positive optical dispersion with diffraction gratings [7] or a fiber to stretch (chirp) the amplifier input pulse before amplification to about a nanosecond duration. After amplification, the stretched pulse is then compressed to a short pulse by a compensating with a negative dispersion system (compressor), using gratings or prisms.

The demonstration of the optical chirped pulse amplification by D. Strickland and G. Mourou in 1985 [4] has opened up the pathway to generate ultra-intense ultra-short pulses. In order to generate ultra-high energy pulses, multiple amplifier

stages are usually required. CPA based Ti:Sapphire laser systems are now commercially available [5] that can produce very high intensity high energy pulses exceeding the PW power level at 800 nm output wavelength. However, the presently available commercial systems are not considered to be the ultimate solution to the generation of ultra-short pulse of ultra-high intensity due to their poor wall plug efficiency below 0.1%. Any practical industrial, scientific or medical applications would require electrical to optical efficiencies of the order of 10% or better. Due to its operation wavelength of 800 nm and very short lifetime of the upper laser level which is only ≈ 3 μs, the Ti:sapphire laser system requires a frequency doubled, flash lamp pumped, Q-switched Nd:YAG laser as pump source. Because of the requirement of such complicated pumping arrangement the Ti:sapphire laser system is quite costly also.

The invention of Yb doped laser media, on the other hand, has quickly drawn the attention of the laser developers because of it strong absorption band near the commercially available diode laser wavelengths. As opposed to flash lamp pumping the direct diode pumping is very efficient. On the other hand the Yttrium aluminum garnet (YAG) is already known as a laser host material which has a very high thermal conductivity and high optical damage threshold [6] and which is very important in the development high intensity laser systems. Therefore, the Yb doped material Yb:YAG has drawn considerable attention as a laser material scalable to high energy and high intensity. Yb:YAG lases at 1030 nm in the infrared wavelength range and can be optically pumped at 940 nm where many commercial diode lasers operate. Therefore, pumping can be carried out using

high power diode lasers which are now commercially available with electrical to optical conversion efficiencies of 60 to 70%. With careful design of such laser diode pumped amplifiers can be operated at optical pump to optical output pulse efficiencies of the order of 20 to 30%, allowing for high power pulsed lasers with overall electrical to optical efficiencies of the order of 10 to 20% as required for industrial applications. Moreover, other studies have shown Yb:YAG to have long upper level life time of the order of milliseconds that will allow efficient pumping to store large amounts of energy. It also has quite high absorption and emission cross sections that will allow the development of systems with very high gain and with very high efficiency [7–11]. Several research groups have already successfully proven the potential of Yb:YAG to be a very strong candidate for the high energy applications including the Max Born Institute of Berlin in Germany [12], the Institute of laser Engineering at Osaka University in Japan [13,14], the LULI Laboratory at Ecole Polytechnique in France [15] and more.

Computer simulations are a very effective to help design and predict the laser system performance. After successful development of a laser model the design parameters can be easily varied saving time and money in the parametric study and optimization of a given system to achieve specified goals.

This thesis presents an experimental and numerical design study of a high efficiency multipass Yb:YAG amplifier stage which can be scaled to high energy applications. Parameters of Yb:YAG published in literature are used to compare with the experimental results. A diode pumped cryogenic laser amplifier system demonstrating very high gain at cryogenic temperature was built and tested.

Problems of transverse ASE or parasitic lasing are explored and an advanced design for a compact and low cost multipass amplifier with a small number of optical components is proposed.

1.2 Previous Work

Ultrafast laser technology has gone through a remarkable advancement over the last few decades [16]. Generation of few-cycle optical pulses at extreme intensities has opened up fundamentally new domains of physics including materials processing [1], high energy particle acceleration [2], x-ray generation [3], fast ignition in laser-driven inertial fusion [17] and many others and may eventually reach the laser intensities where particle production in vacuum will occur [18]. The term ultra-short pulse is not very well defined. Often laser pulses ranging from femtoseconds to picoseconds duration are considered to be ultrashort pulses [19]. Ultrafast laser oscillators are often referred to as modelocked lasers since a wide bandwidth of laser modes are locked together to generate the short pulse [16,19]. Ultrashort pulses of picoseconds duration were first experimentally demonstrated by Maria, Stetser and Heynau at United Aircraft Research Laboratories in 1966 [20] only six years after the first demonstration of the laser [21]. The analytic theories of active modelocking were proposed by Kuizenga and Siegman in 1970 [22,22]. Three years after that, the theories of passive mode locking with slow and fast saturable absorbers were published by Haus and co-authors [23,24]. The spectroscopic and laser characteristics of Ti:sapphire were published by Moulton in 1986 [25]. Just a year after, the concept of chirped pulse amplification (CPA) was demonstrated by D.

Strickland and G. Mourou [4]. A large amount of research has been conducted after that to implement the technique in many different laser systems and CPA based Ti:sapphire systems have been commercially available for over two decades [5]. However the main drawback to date in generating ultra-short ultra-intense laser pulse is the cost and the efficiency of such Ti:sapphire systems. The very short life of the upper laser level and the requirement of frequency doubled, flash lamp pumped, Q-switched Nd:YAG lasers as pump sources make the system inefficient, complex and costly. Therefore scientists have been constantly searching for alternative solutions. The demonstration of coherent light emission from semiconductors diode, commonly known as laser diodes by Robert N. Hall [26] and Marthal Nathan [27] in 1962 has opened up new opportunity of direct diode pumping of lasers. The much narrower bandwidth of the laser diode compared to flash lamps offers very high optical pumping efficiency, reduced thermal heating and compact size of the systems. The absorption bands of different rare earth materials such as ytterbium doped crystals and ceramics line up with efficient laser diode emission wavelengths [28,29]. Moreover, Yb doped materials offer large absorption and emission bandwidths with long fluorescence lifetimes on the order of ~1ms [7,10,11,29–32]. Therefore, Yb doped materials have drawn great deal of attention from high power laser facilities around the world during the last decade. The Mercury laser at the Lawrence Livermore National Laboratory in US has been built based on Yb:S-FAP slabs. The cryogenic operation of this laser system produces 55 J, 14 ns pulses at 10 Hz repetition rate [33]. The POLARIS laser is a Yb:FP15 glass based system at the

Institut für Optik und Quantenelektronik, FSU Jena in Germany and produced reported energies upto 4 J in 164 fs pulses at 0.025 Hz [34]. The MBI Disk Laser at the Max Born Institut, Berlin in Germany has a reported output of 320 mJ at 100 Hz rate using a Yb:YAG thin disk configuration [12]. The Lucia system at the Laboratoire LULI, Ecole Polytechnique in France produces 14 J, 8 ns pulses at 2 Hz from Yb: YAG by direct three stage amplification [15]. An overview of the status of the high energy laser system is shown in figure 1.1.

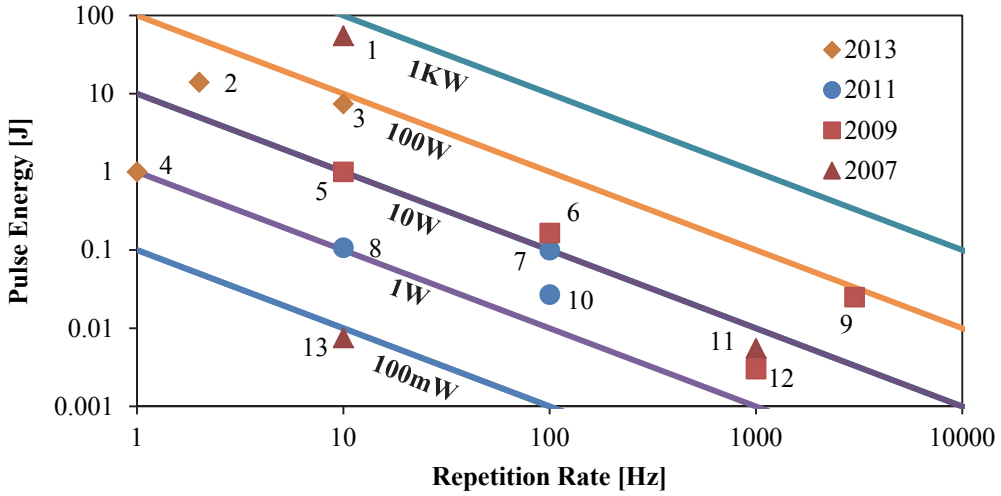

Figure 1.1: Current status of the Yb based high energy laser system. 1: [33], 2: [15], 3: [35], 4: [36], 5: [3], 6: [12], 7: [37], 8: [38], 9: [39], 10: [40], 11: [41], 12: [31], 13: [42]

Chapter 2 Theoretical Background

This chapter is written following the description of the theory lasers in reference [43] by W. Koechner and M. Bass.

2.1 Concept of Laser

The acronym "Laser" stands of Light Amplification by Stimulated Emission of Radiation. The concept of stimulated emission was first proposed by Albert Einstein in 1917 [44]. The concept can be described in simplified fashion as follows. If we consider an idealized material with just two nondegenerated energy levels, 1 and 2 as shown in figure 2.1, having populations of N_1 and N_2 respectively, assuming the total number of atoms in the system to be constant, we can write,

$$N_1 + N_2 = N_{tot} \qquad (1)$$

The difference in energy between the levels are

$$E_2 - E_1 = h\nu_{21} \qquad (2)$$

where h is the Planck's constant, $\nu_{21}$is the frequency. The atom can transfer from E_2 state to the ground state E_1 by emitting a photon of energy $h\nu_{21}$ and conversely, can transfer from E_1 state to E_2 state by absorbing the same amount of energy. Therefore we can expect three possible events from such an atomic system namely absorption, spontaneous emission and stimulated emission.

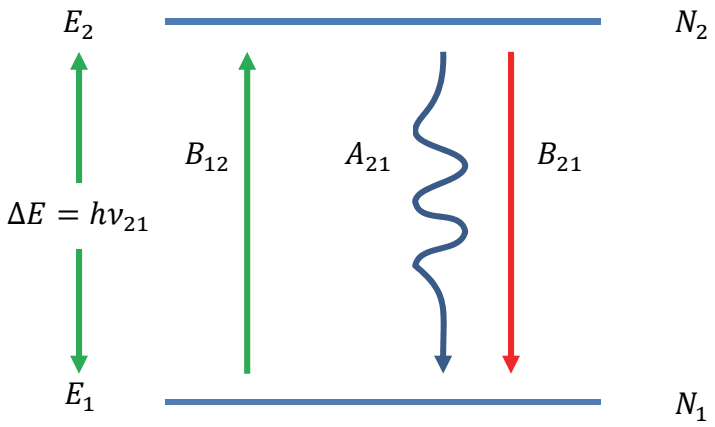

Figure 2.1: Energy level schematic of a two level system

2.1.1 Absorption

If an electromagnetic wave of frequency ν_{21}passes through the above system, the population of the lower level will be depleted at a rate proportional to the radiation density, $\varrho(\nu)$ and the rate of change of the population N_1 of that level is given by,

$$\frac{\partial N_1}{\partial t} = -B_{12}\varrho(\nu_{21})N_1 \qquad (3)$$

where B_{12} is a constant of proportionality with dimensions cm^3/s^2 J.

2.1.2 Spontaneous Emission

After an atom has been raised to the upper level by absorbing external energy, the population of the upper level will decay spontaneously to the lower level at a rate proportional to the upper level population given by,

$$\frac{\partial N_2}{\partial t} = -A_{21}N_2 \qquad (4)$$

where $A_{21}$is a constant of proportionality with dimension s^{-1}. Since this is a phenomena that is independent of external influence, equation (4) can be solved independently with a solution as follows,

$$N_2(t) = N_2(0)\exp\left(-\frac{t}{\tau_{21}}\right) \tag{5}$$

where $\tau_{21} = A_{21}^{-1}$ is the life time for spontaneous radiation of level 2.

2.1.3 Stimulated Emission

In this case, the emission takes place under the stimulation by electromagnetic radiation of the appropriate frequency. The phenomena is modeled by,

$$\frac{\partial N_2}{\partial t} = -B_{21}\varrho(\nu_{21})N_2 \tag{6}$$

where B_{21} is a constant of proportionality.

2.2 Derivation of Rate Equations

2.2.1 Two Level System

By combining all the equations (1)-(6) the upper and the lower level populations can be related as,

$$\frac{\partial N_1}{\partial t} = -\frac{\partial N_2}{\partial t} = B_{21}\varrho(\nu_{12})N_2 - B_{12}\varrho(\nu_{12})N_1 + A_{21}N_2 \tag{7}$$

Under thermal equilibrium,

$$\frac{\partial N_1}{\partial t} = -\frac{\partial N_2}{\partial t} = 0 \tag{8}$$

Therefore, we can write

$$B_{21}\varrho(\nu_{12})N_2 + A_{21}N_2 = B_{12}\varrho(\nu_{12})N_1 \qquad (9)$$

In an isothermal enclosure or cavity, the radiation density $\varrho(\nu)d\nu$ at thermal equilibrium temperature T is given by the Planck's law as,

$$\varrho(\nu)d\nu = \frac{8\pi\nu^2 d\nu}{c^3}\frac{h\nu}{\exp(h\nu/kT) - 1} \qquad (10)$$

where h is the Planck's constant, k is the Boltzmann's constant, c is the velocity of light.

In thermal equilibrium the statistical distribution of the population can be calculated using the Boltzmann equation,

$$\frac{N_2}{N_1} = \exp\left(-\frac{E_2 - E_1}{kT}\right) \qquad (11)$$

where k is the Boltzmann constant and T is the temperature.

Using the Boltzmann distribution in equation (9) for the ratio N_2/N_1, we get,

$$\varrho(\nu_{12}) = \frac{(\mathrm{A}_{21}/\mathrm{B}_{21})}{(B_{12}/B_{21})\exp\,(h\nu_{12}/kT) - 1} \qquad (12)$$

Now comparing it to the Planck's blackbody radiation, the Einstein's coefficients can be written as,

$$\frac{A_{21}}{B_{21}} = \frac{8\pi\nu^2 h\nu}{c^3} \quad \text{and} \quad B_{12} = B_{21} \qquad (13)$$

To derive the rate equations for the simulation, we need to express the probability for the stimulated emission,$\varrho(\nu)B_{21}$ in terms of measurable quantity such as

photon density, ϕ and the stimulated emission cross section, σ_{21}. Therefore we can write,

$$B_{12} = B_{21} = \frac{c}{h\nu}\sigma \tag{14}$$

The energy density can be written as,

$$\varrho(\nu) = h\nu\phi \tag{15}$$

where ϕ is the photon density. For single frequency operation or vary narrow band input electromagnetic wave we can drop the lineshape function, $g(\nu)$. The lineshape function can be defined as the probability of emission or absorption per unit frequency. Therefore, combining all the equations above we can model a two level system using the following rate equations

$$\frac{\partial N_1}{\partial t} = -\frac{\partial N_2}{\partial t} = \sigma c(N_2 - N_1)\phi \tag{16}$$

Each transition from N_2 to N_1 will result in emission of a photon and absorption for the reverse transition. Therefore the photon flux density can be written as,

$$\frac{\partial \phi}{\partial t} = \frac{\partial N_1}{\partial t} = -\frac{\partial N_2}{\partial t} = \sigma c\phi(N_2 - N_1) \tag{17}$$

The space dependency of the equations can be derived from the definition of the speed of light i.e. the electromagnetic wave velocity, $c = dz/dt$. Therefore, the space dependent photon flux density rate equation can be written as,

$$\frac{\partial \phi}{\partial z} = \sigma(N_2 - N_1)\phi \tag{18}$$

Therefore the photon transport equation of a two level system can be written as,

$$\frac{\partial \phi}{\partial t} + c\frac{\partial \phi}{\partial z} = \sigma c \phi (N_2 - N_1) \qquad (19)$$

In the absence of incident wave, the population distribution in thermal equilibrium depends on the Boltzman distribution law. Therefore in two level system N_2 is less than N_1 in the absence of an incident wave. The incident radiation will therefore be absorbed until $N_1 = N_2$ where the absorption rate is equal to the emission rate. Therefore, population inversion is not possible in a two level system. This means to build a laser we need more complex material having multiple energy levels.

2.2.2 Three Level System

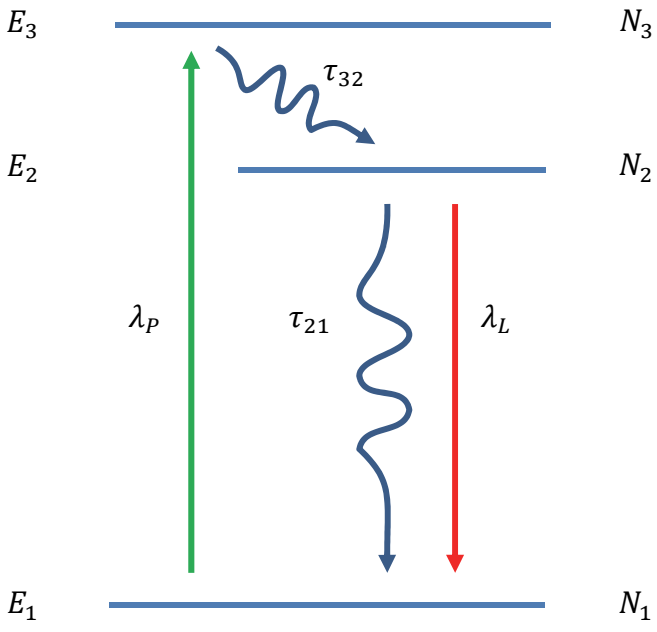

Figure 2.2: Energy level schematic of a three level system

In a three level system as shown in figure 2.2, an incident pump wave of frequency $\nu_P = c/\lambda_P$ is chosen so that the transition occurs from the energy level 1 to level 3. The population then decays from level 3 to level 2 at a rate of $1/\tau_{32}$. Finally this state decays from level 2 to level 1 giving away energy in the form of electromagnetic wave of wavelength, λ_L at a rate of $1/\tau_{21}$. If $\tau_{32} \ll \tau_{21}$, the N_3 state will be depopulated very quickly and we will be able to assume $N = N_1 + N_2$. Thus we can simplify the model to a two level system except population inversion will be possible. The population inversion will be achieved when $N_2 > N/2$. Once the population inversion is achieved, amplification of the incident radiation will be possible.

2.2.3 Four Level System

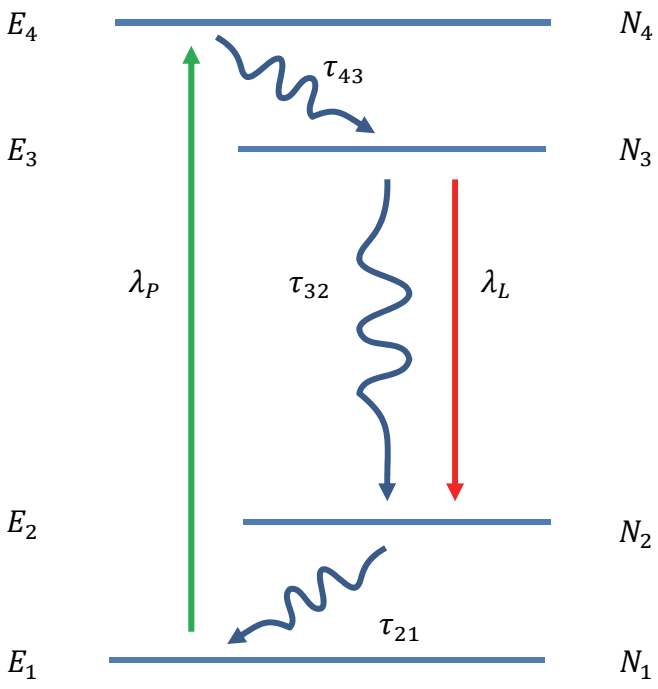

Figure 2.3: Energy level schematic of a four level system

The three level system requires a very high pump rate to achieve population inversion. In the four level system on the other hand the population inversion is possible with very low pumping rate. A four level system is shown in figure 2.3. In the four level laser system we require $\tau_{43} \ll \tau_{32}$ and $\tau_{21} \ll \tau_{32}$. The main advantage of the four level system over three level system is that the lower laser level (second level) is always empty due to the fact that $\tau_{21} \ll \tau_{32}$. If the pump wavelength is chosen to be λ_P the transition occurs directly from the ground state to the fourth level and decays from fourth level to the third level at rate of $1/\tau_{43}$. The third level is the laser upper level. Since the lower laser level is empty, all the population of the third level will contribute to the amplification of the incident radiation. Although Yb:YAG is a quasi-three level system at room temperature, it behaves like a four level system at cryogenic temperature.

2.2.4 Quasi Three Level System

If the lower laser level of a four level system is very close to the ground state i.e. the lower laser level is on the order of few $\approx kT$ from the ground state, the lower laser level gets thermally populated even at room temperature. This kind of system behaves neither like a four level system nor like a three level system. To provide amplification, quasi three level systems requires $N_2 > N_{10}$ given by the thermal population N_{10} of the lower level which means that they cannot be pumped as easily as a four level system. This kind of system is quite temperature dependent and can behave like a four level system at cryogenic temperature and like a three level laser at elevated temperatures. Yb:YAG is one example of a

quasi-three level system that we have studied as a gain medium for a high performance laser amplifier.

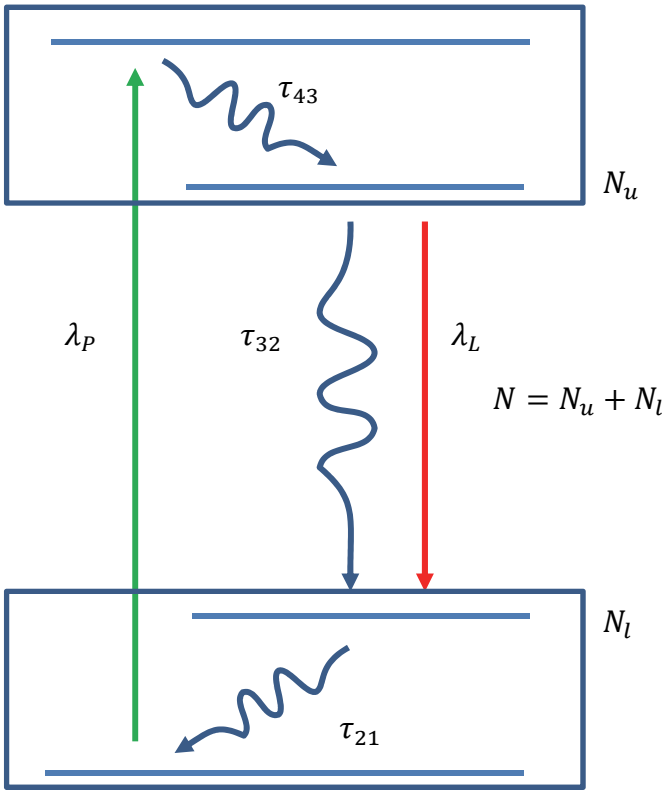

Figure 2.4: Energy level schematic of a four level system

The rate equations of a quasi three level system can be modeled as a two level system we have discussed in section 2.2.1 with some minor modifications. If we assume $\tau_{43} \ll \tau_{32}$ the time dependent population of the upper laser level can be calculated as,

$$\frac{dN_u}{dt} = \sigma_P c\phi(N - N_u) - \frac{N_u}{\tau_u} \qquad (20)$$

where σ_P is the absorption cross-section at pump wavelength.

If we use the relation between the photon flux density with the pump intensity, $I_P = ch\nu_P\phi$, we get,

$$\frac{dN_u}{dt} = \frac{\sigma_P}{h\nu_P}(N - N_u)I_P - \frac{N_u}{\tau_u} \tag{21}$$

The absorption of pump and the population of the upper laser level is calculated by solving the above equation numerically. In case of no spontaneous emission or when the upper level lifetime is very large, we can drop the second part of the right hand side of the above equation and model the pure pump absorption by the gain medium.

$$\frac{dN_u}{dt} = \frac{\sigma_P}{h\nu_P}(N - N_u)I_P \tag{22}$$

The analytical solution to this equation is given by,

$$N_u = N\left(1 - \exp\left(-\frac{\sigma_P}{h\nu_P}I_P t\right)\right) \tag{23}$$

If we rewrite he equation in terms of pump fluence, $F_P = I_P t$ then the above equation becomes,

$$N_u = N\left(1 - \exp\left(-\frac{\sigma_P}{h\nu_P}F_P\right)\right) \tag{24}$$

If we define a variable called pump saturation fluence as,

$$F_{sat} = \frac{h\nu_P}{\sigma_P} \tag{25}$$

Then equation (24) becomes,

$$N_u = N\left(1 - \exp\left(-\frac{F_P}{F_{psat}}\right)\right) \tag{26}$$

According to the above equation, when the pump fluence is larger than the saturation fluence, the upper level approaches the maximum value of N. Pumping the gain medium with very high pump fluence will allow a uniform population inversion over the crystal length. However, too high pump fluence may damge the medium. The absorbed pump energy can be modeled according to equation (19) as,

$$\frac{\partial \phi_P}{\partial t} + c\frac{\partial \phi_P}{\partial z} = c\sigma_P \phi_P (N - N_u) \tag{27}$$

This equation can also be written in terms of pump intensity as,

$$\frac{\partial I_P}{\partial t} + c\frac{\partial I_P}{\partial z} = c\sigma_P I_P (N - N_u) \tag{28}$$

If the medium is irradiated with a square pulse in time of pulse width, T_P then equation (22) and (28) can be written in terms of pump fluence as,

$$\frac{dN_u}{dt} = \frac{(N - N_u)}{T_P}\frac{F_P}{F_{sat}} \tag{29}$$

$$\frac{\partial F_P}{\partial t} + c\frac{\partial F_P}{\partial z} = c\sigma_P F_P (N - N_u) \tag{30}$$

Now equation (29) and (30) can be solved numerically for pump absorption and population inversion as shown in figure 2.5.

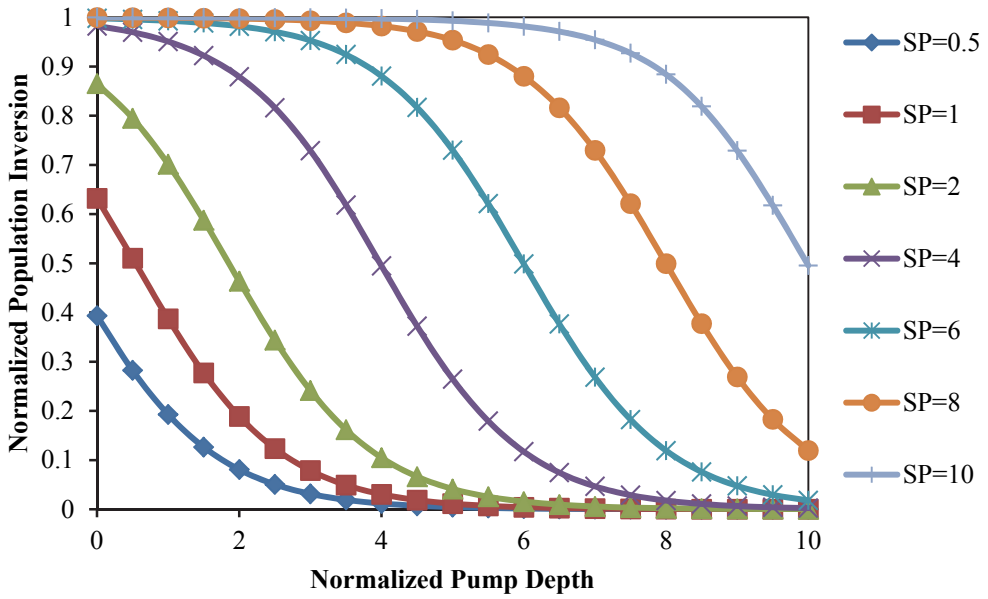

Figure 2.5: Population inversion profile at different pump fluences to show the significance of the saturation fluence on the pump absorption. Here, $SP = F_P/F_{sat}$. The normalized population inversion is defined as N_u/N and the pump depth is normalized with respect to the small signal absorption length, $L_A = 1/(N\sigma_P)$

The laser pulse amplification can be modeled according to equation (19) as,

$$\frac{\partial I_L}{\partial t} + c\frac{\partial I_L}{\partial z} = c\sigma_L I_L N_u \qquad (31)$$

The depletion of the upper state population as the pulse is amplified can be modelled according to equation (17) as,

$$\frac{\partial N_u}{\partial t} = c\sigma_L I_L N_u \qquad (32)$$

The coupled equations (31) and (32) can be solved numerically to calculate the pulse growth inside the medium. An analytical solution is derived by Frantz and Nodvik [45] as,

$$I_L(z,t) = \frac{I_0}{\left\{1 - [1 - \exp(-\sigma_L N_u z)] \exp\left[c\sigma_L I_L\left(t - \frac{z}{c}\right)\right]\right\}} \quad (33)$$

where, I_0= initial laser intensity. The photon flux densities in Frantz and Nodvik equation have been replaced with the equivalent light intensities to maintain the consistency with our derived equations. This equation can be rewritten in term of pulse fluence for simulation purpose as,

$$F_{out} = F_{sat} \ln\left[1 + \left\{\exp\left(\frac{F_{in}}{F_{sat}}\right) - 1\right\} \exp\left(\frac{F_{st}}{F_{sat}}\right)\right] \quad (34)$$

where, F_{st} is the stored fluence and F_{sat} is the laser saturation fluence given by,

$$F_{st} = h\nu_L N_u \quad (35)$$

and

$$F_{sat} = \frac{h\nu_L}{\sigma_e} \quad (36)$$

where $h\nu_L$ is the energy per laser photon and σ_e is the emission cross-section.

2.3 Yb:YAG Ceramic as Gain Medium

Several Yb doped materials have been investigated over the last decade. A very good comparison of different Yb doped materials can be found in the references [10,11,29,46,47]. The choice of laser gain medium depends on many factors such as the absorption and emission peak wavelengths and bandwidth, fluorescence lifetime, saturation fluence, damage threshold, thermal conductivity, etc. To generate short pulses, a large emission bandwidth is needed. The large absorption bandwidth gives more freedom to choose the pump wavelength hence pump diode. A long fluorescence lifetime allows more storage of energy for a given

pump power and leads to more cost effective pumping. High emission peak cross-section results in a lower saturation fluence that allows more efficient extraction of energy at lower fluences. However, very low saturation fluence also allows more energy loss through ASE. For a high intensity system, a high damage threshold is also a requirement. At high intensity the laser gain medium gets heated up very quickly. Therefore, high thermal conductivity will allow efficient heat extraction avoiding thermal damage or shock of the gain medium. We have chosen Yb:YAG as our gain medium because of the large absorption bandwidth with high peak near 940 nm [11], high emission peak with moderate bandwidth near 1030 nm [11], high thermal conductivity [46,47], and high damage threshold [6,48].

Chapter 3 Modeling of Yb:YAG Amplifier

3.1 System Modeling

It is clear from the energy level scheme shown in figure 3.1 that the pump wavelength for Yb:YAG can be chosen among $10930\ \mathrm{cm}^{-1}$ (915 nm), $10624\ \mathrm{cm}^{-1}$ (941 nm) or $10327\ \mathrm{cm}^{-1}$ (968 nm) absorption lines from the ground level.

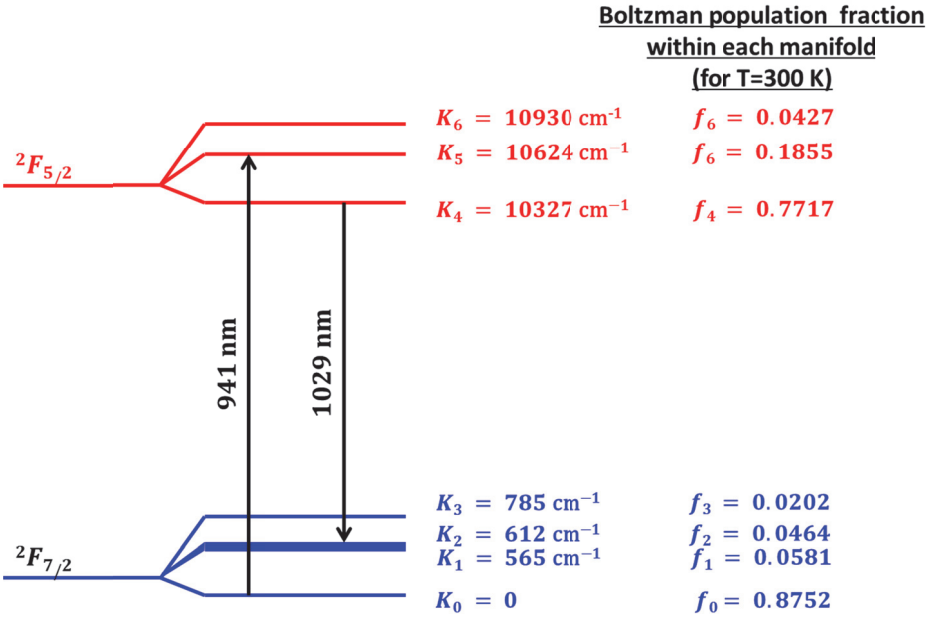

Figure 3.1: Energy level scheme of Yb:YAG (according to [9,49])

The absorption cross-section in figure 3.2 shows strong absorption peaks at 941 nm and 968 nm with FWHM bandwidths of 18 nm and 4 nm respectively [8]. The broad absorption band, high absorption peak near 941 nm and the availability of high efficiency commercial diode lasers near 940 nm makes this wavelength more favorable for pump the laser crystal. The seed laser wavelength has to be around 1029 nm in wavelength to get the maximum gain from Yb:YAG crystal because

of the peak in emission cross-section at this wavelength. It is also observed from figure 3.2 that both the absorption and emission cross-sections are highly temperature sensitive and the emission cross-section increase significantly as the crystal is cooled. Therefore, to design an amplifier with very high gain, the crystal can be cooled to cryogenic temperature.

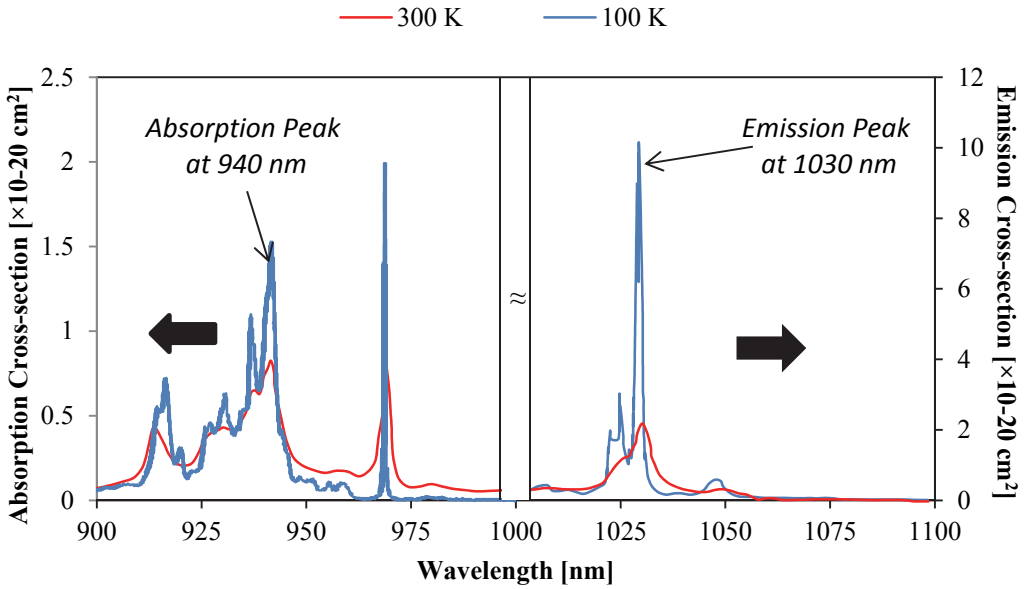

Figure 3.2: Absorption and emission cross-section of Yb:YAG (Reproduced from [10])

Another important property of Yb:YAG can be derived by observing the energy level diagram more closely. The energy level diagram indicates that the ground level and the lower laser level are located on the same manifold $^2F_{7/2}$. Similarly, the chosen pump energy level and the upper laser level are located at the same manifold $^2F_{5/2}$. Because of the small separation of energy levels in the same manifold, an increase in temperature can result in significant populations in all levels of the manifold. Therefore it is important to calculate the thermal occupation density of each energy level for modeling the Yb:YAG as a gain

medium at room temperature. The thermal occupancy can be calculated using the Boltzmann distribution function. The thermal occupancy distribution within a manifold of different energy levels is given by [49],

$$f_i = \frac{\exp\left(-\frac{k_i hc}{T\kappa_b}\right)}{\sum_j \exp\left(-\frac{k_j hc}{T\kappa_b}\right)} \qquad (37)$$

where k_i and k_j denote the wave number for the different levels with regard to the ground level, h and c are the Plank constant and velocity of light in vacuum, T stands for the temperature of the laser medium, and κ_b is the Boltzmann constant. For the lower levels, the values of f_i $(i = 0 - 3)$ are calculated with the summation of $j = 0 - 3$, and for the upper levels, the values of $f_i (i = 4 - 6)$ are calculated with the summation of $j = 4 - 6$, respectively. The calculated thermal occupancy using equation (37) for different temperatures are listed in table 3.1.

Table 3.1: Thermal occupancy fractions or Boltzmann Population fractions at different temperature [9,49]

Boltzmann Population	At 0 K	At 77 K	At 100 K	At 200 K	At 300 K
f_0	1	0.999963	0.999546	0.968199	0.875223
f_1	0	0.000025	0.000293	0.016578	0.058144
f_2	0	0.000010	0.000148	0.011819	0.046403
f_3	0	4.22079×10^{-7}	0.000012	0.003402	0.020229
f_4	1	0.996128	0.986128	0.884243	0.771735
f_5	0	0.003859	0.013704	0.10424	0.185542
f_6	0	0.000012	0.000167	0.011517	0.042722

The data from Table 3.1 indicates that Yb:YAG basically can be modeled as a four level laser at lower temperature (below ~100K) because at low temperature, the lower laser level f_1 remains almost empty and the excited electrons mostly occupy the f_4 state which is the upper laser level. Therefore, the most efficient population inversion is achieved and the laser works as a four level laser at such cryogenic temperatures. However, at room temperature, the situation is different. At this temperature, the values in table 3.1 indicate a significant amount of occupancy at the lower laser level and a fraction of the upper laser level electrons are thermally excited to higher energy levels. Therefore, the population inversion and the pump efficiency are significantly reduced at this temperature for a given pump power.

3.1.1 System Model for Matlab

The absorbed pump power at any temperature can be calculated if the absorption cross section is known. The absorbed pump intensity of a laser medium can be calculated as [49],

$$P_{abs} = P_{pump}\left[1 - \exp\left\{-\sigma_P\left(f_0 N_{d_L} - f_5 N_{u_L}\right)\right\}\right] \quad (38)$$

Where, P_{abs} is the absorbed pump power, P_{pump} is the launched pump power, σ_P is the absorption cross section, N_{u_L} is the line integrated population of the upper manifold, and N_{d_L} is the line integrated population of the laser active ions in the host. Although Yb:YAG laser is a quasi three-level or quasi four-level system, for modeling purpose, the system can be treated as a two level system under the assumption that there are fast relaxations between the levels within one manifold

compared to the fluorescence lifetime [9]. For very short pulse energy extraction, it would be more appropriate to consider the system as a four level system where the transitions between the energy level within the same manifold are also considered. However, the two level assumptions shows good agreement with the experimentally measured values for pulse widths of the order of 1 ps to 10 ns in a number of previous studies [9,10,49–62]. Therefore, we have used the simplified two level model to predict the performance of the Yb:YAG system.

We have already calculated the absorbed pump power in equation (38). This pump power excites a line integrated population of $N_{u_L} = P_{abs}/h\nu_P$ per unit time in the pump energy level of $^2F_{5/2}$ manifold. N_{u_L}/τ_u is the decay rate of the line integrated upper level population where τ_u is the upper state fluorescence lifetime. Therefore, the total increase in population in the line integrated upper energy level population per unit time becomes [49]

$$\frac{dN_{u_L}}{dt} = \frac{P_{abs}}{h\nu_P} - \frac{N_u}{\tau_u} \tag{39}$$

Equation (39) calculates the population achieved only from the pump. The line integrated population inversion can be calculated from,

$$\Delta N_L = f_4 N_{u_L} - f_2\left(N_{d_L} - N_{u_L}\right) \tag{40}$$

Therefore, the stored fluence is,

$$F_{st} = h\nu_L \Delta N_L \tag{41}$$

where $h\nu_L$ is the energy per laser photon.

The small signal gain co-efficient of the laser rod is therefore,

$$g_0 l = \sigma_e \Delta N_L \tag{42}$$

where, l is the length of the laser medium and σ_e is the emission cross section. The saturation fluence can be calculated from,

$$F_{sat} = \frac{h\nu_L}{\sigma_e} \tag{43}$$

Now combining equation (40)-(43) the small line integrated signal gain can be expressed as a ratio of the stored fluence and the saturation fluence,

$$g_0 l = \frac{F_{st}}{F_{sat}} \tag{44}$$

The amplifier output after the nth pass can now be calculated using the Frantz-Nodvik equation for output for the nth pass, [49]

$$F_{out}^{(n)} = F_{sat} \ln\left[1 + \left\{\exp\left(\frac{F_{in}^{(n)}}{F_{sat}}\right) - 1\right\}\exp\left(\frac{F_{st}^{(n)}}{F_{sat}}\right)\right] \tag{45}$$

and updating the stored energy and laser energy fluence for the (n+1) th pass

$$F_{st}^{(n+1)} = F_{st}^{(n)} - \left(F_{out}^{(n)} - F_{in}^{(n)}\right)(f_2 + f_4) \tag{46}$$

$$F_{in}^{(n+1)} = (1 - Loss)F_{out}^{(n)} \tag{47}$$

Where $F_{in}^{(n)}$ and $F_{out}^{(n)}$ denote the input and output of the laser pulse fluencies for the nth pass, $Loss$ is the loss of the resonator per single pass.

However, in the Frantz-Nodvik equation there is no explicit absorption term at the laser wavelength. Previous experiments and our experimental results have shown

that there is significant amount of absorption at 1030 nm. Therefore, this absorption term is included in the form of a transmission factor in equation (45). The transmission factor at 1030 nm in Yb:YAG can be modelled as,

$$T_{abs_{1030}} = \exp(-\sigma_{a_{1030}} N_l l) \tag{48}$$

where $\sigma_{a_{1030}}$ is the absorption cross-section, l is the crystal length, and $N_l = N_d - N_u$ is the line integrated population of the lower level. Therefore, the modified Frantz-Nodvik equations become,

$$F_{out}^{(n)} = T_{abs_{1030}} F_{sat} \ln\left[1 + \left\{\exp\left(\frac{F_{in}^{(n)}}{F_{sat}}\right) - 1\right\} \exp\left(\frac{F_{st}^{(n)}}{F_{sat}}\right)\right] \tag{49}$$

$$F_{st}^{(n+1)} = F_{st}^{(n)} - \left(F_{out}^{(n)} - F_{in}^{(n)}\right)(f_2 + f_4) \tag{50}$$

$$F_{in}^{(n+1)} = (1 - Loss) F_{out}^{(n)} \tag{51}$$

However, as we have seen before that the Yb:YAG cross-sections are very temperature sensitive, it is important to consider the effect of heating of the crystal during operation too. A very good feature of Yb:YAG is its quantum defect is small which can be calculated as follows [63],

$$\eta_q = 1 - \frac{\lambda_p}{\lambda_l} = 0.087 \tag{52}$$

It means that only 8.7% of the absorbed pump will contribute to the heat generation. Then the conventional heat equations can be used to calculate the increase in temperature [64].

$$\rho C \frac{\partial T(x,y,z,t)}{\partial t} - K\nabla^2 T(x,y,z,t) = Q(x,y,z,t) \qquad (53)$$

Here K is the thermal conductivity of Yb:YAG, ρ is the density, C is the specific heat capacity and Q is the thermal power density of the heat source (the fraction of the absorbed pump). Equations (38)-(44) and (48)-(51) are then solved first in Matlab for a uniform planewave with no change in diameter without considering the effect of geometry. The same equations are then solved in COMSOL Multiphysics 4.3 to consider the effect of the geometric overlap of pump and laser beams.

3.1.2 System Model for COMSOL

To model the system in COMSOL, we needed to rewrite the equations in differential form as derived in [65]. Equation (38) is modelled in terms of remaining pump power as it propagates through the gain medium as follows.

$$\frac{\partial I_P}{\partial t} + c.(\nabla I_P) = \sigma_P c(f_0 N_d - f_5 N_u) I_P \qquad (54)$$

Here, c is the speed of light and I_P is the pump intensity. Equation (39) and (40) are kept unchanged. In this case, the population values are not line integrated.

$$\frac{dN_u}{dt} = \frac{P_{abs}}{E_{PP}} - \frac{N_u}{\tau_u} \qquad (55)$$

$$\Delta N = f_4 N_u - f_2(N_d - N_u) \qquad (56)$$

Pulse amplification is calculated using the following equations

$$\frac{\partial I_L}{\partial t} + c.(\nabla I_P) = -\sigma_e c \Delta N \, I_P \qquad (57)$$

Theses equations along with the supporting equations from the previous section are solved on a 3D spatial grid in COMSOL with the proper boundary conditions to simulate the amplifier operation.

3.2 Simulation parameters

Aggarwal [66] measured the density of YAG, $\rho = 4.56\ \mathrm{g/cm^3}$. The molecular mass of YAG ($Y_3Al_5O_{12}$) is $M = 593.7\ \mathrm{g/mol}$ [67].

∴ YAG number density, $N_{YAG} = \frac{N_A \times \rho}{M} = 4.6 \times 10^{21}$ per $\mathrm{cm^3}$

At 10% doping, Yb^{3+} number density, $N_{Yb} = 0.1 \times 3 \times N_{YAG} = 1.38 \times 10^{21}$ per $\mathrm{cm^3}$

If we calculate the absorption cross-sections of the Yb:YAG crystal of different doping concentration at 940 nm wavelength from the absorption coefficient spectrum measured by Dong et. al. in [7] we will find that the absorption co-efficient changes with the doping concentration but absorption cross-sections do not. Two examples are given below.

At 10% doping, the absorption co-efficient is $11.1\ \mathrm{cm^{-1}}$ [7]. Therefore, the absorption cross section,

$$\sigma_A = \frac{11.1}{0.1 \times 3 \times N_{YAG}} = 0.80435 \times 10^{-20}\ \mathrm{cm^2} \approx 0.8 \times 10^{-20}\ \mathrm{cm^2}$$

Similarly at 5% doping, the absorption co-efficient is $5.55\ cm^{-1}$ [7]. Therefore, the absorption cross section,

$$\sigma_A = \frac{5.55}{0.05 \times 3 \times N_{YAG}} = 0.80435 \times 10^{-20}\mathrm{cm^2} \approx 0.8 \times 10^{-20}\mathrm{cm^2}$$

Although the absorption cross-sections do not depend on the doping concentration they are very temperature sensitive as shown in figure 3.2. Therefore, temperature dependent emission cross-section values are used for the gain calculation. To consider the temperature dependency, a polynomial fit through the measured absorption and emission cross-section data reported in the literature is used. A polynomial fit of absorption cross-section is obtained through the data reported in references [10,11] is shown in figure 3.3. For the emission cross-section the polynomial fit reported in reference [7] was used directly as shown in figure 3.4.

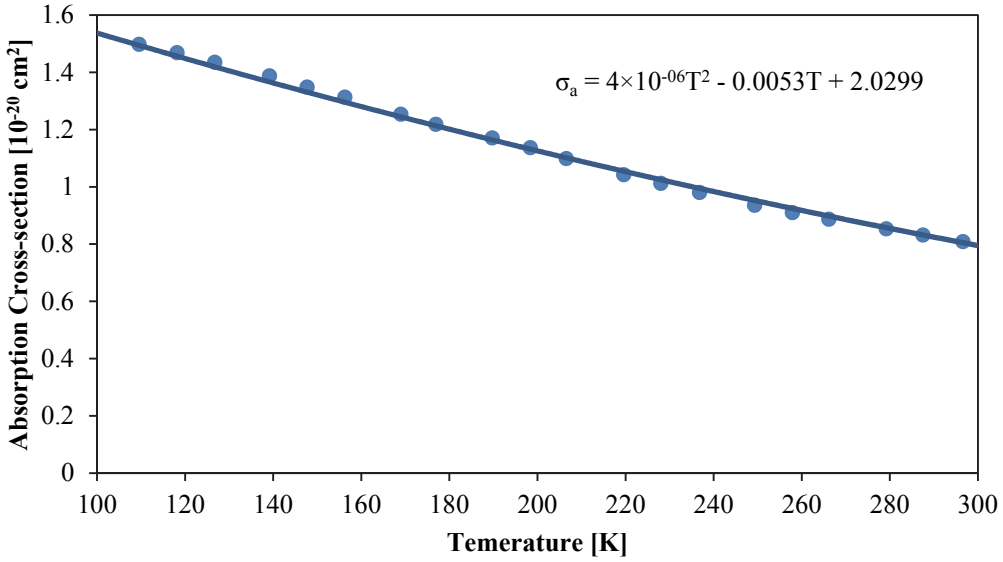

Figure 3.3: Polynomial fit to temperature dependent peak absorption cross-section at 940 nm (Measured values (dots) are taken from [10,11])

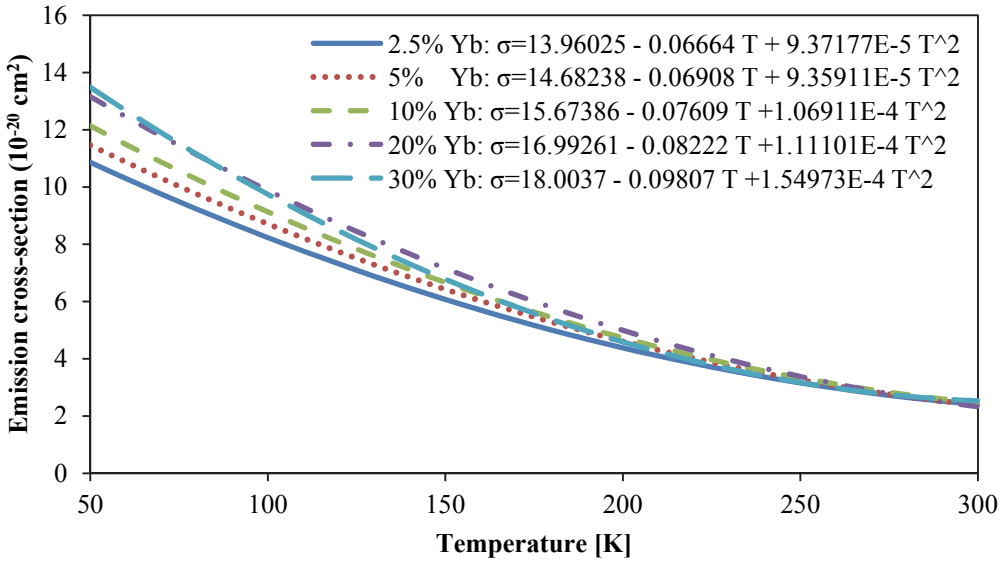

Figure 3.4: Polynomial fit to temperature dependent peak emission cross-sections at 1030 nm taken from [7]

The heat capacity and the thermal conductivity are $620\,\mathrm{J\,kg^{-1}K^{-1}}$ and $5.7\,\mathrm{W\,m^{-1}\,K^{-1}}$ respectively [66]. The Yb:YAG parameters are summarized in table 3.2.

Table 3.2: General Parameters of Yb:YAG

General Yb:YAG Parameters	
YAG concentration [9,49,68]	4.6×10^{21} per $\mathrm{cm^3}$
Yb concentration at 10% doping	1.38×10^{21} per $\mathrm{cm^3}$
Absorption Wavelength [7–11]	941 nm
Emission Wavelength [7–11]	1029 nm
Absorption Cross Section at 300 K [7–11]	0.8×10^{-20} $\mathrm{cm^2}$
Emission Cross Section at 300 K [7–11]	2.3×10^{-20} $\mathrm{cm^2}$
Upper State Lifetime [7–11]	951 µs

3.3 Simulation in Matlab

After performing some initial experiments that will be discussed in 4.2 we have decided to build system similar to the system of the Colorado State University group reported in [3,37]. Therefore as a first test we have tried to compare our model output to the measured output of their system. Firstly we have simulated the room temperature behavior and then the cryogenic behavior reported in [37] and [3] respectively.

3.3.1 Description of the model

Equations (38)-(44) and (48)-(51) are first solved in Matlab using the system parameters published in the literature to check the validity of our model.

At first, the pump absorption and the population inversion is calculated using equations (37)-(40). To calculate the penetration depth of the pump and the time dependent nonlinear distribution of the population inversion, we have divided the crystal into multiple segments and treated each segment to be an independent laser crystal. The transmitted pump from each segment is considered to be the input pump for the next segment. An example of the results obtained are shown in figure 3.5 where the time evolution of the population inversion is shown along the pump beam inside a crystal 5 mm thick Yb:YAG crystal pumped at $200\ \mathrm{kW/cm^2}$ for 1ms. Although the total energy fluence of $200\ \mathrm{J/cm^2}$ is above the damage threshold [69] of the YAG gain medium the example is given to show that the model can display the bleaching effects properly. Such high pump thresholds are

possible inside the laser crystals since Binh [6] has reported the single pulse internal damage threshold is 1400 J/cm^2 for 9.9 ns long pulses.

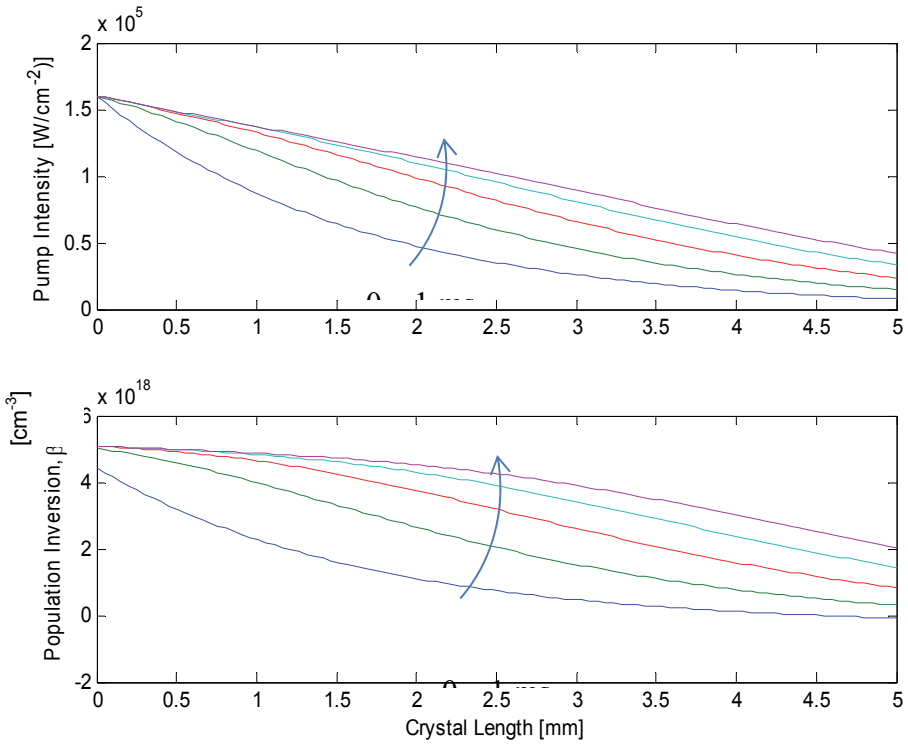

Figure 3.5: Time evolution of pump absorption and population inversion for a pump intensity of 200 kW/cm^2 at a wavelength of 940 nm shown for times of 0.2, 0.4, 0.6, 0.8 and 1.0 ms from bottom to top

Equation (41)-(44) and (48)-(51) are then solved to calculate the energy extraction. These equations are then solved along several parallel lines in the direction of the laser beam to calculate the laser beam size and the extraction efficiency. The parallel grid lines are setup along the thickness of the gain medium parallel to the beam propagation direction. For a high resolution beam profile, 50 grid lines per axial direction are setup that gives 2500 gridlines along the thickness of the gain medium. An example of change in laser beam size

illustrating multipass saturated extraction of a high gain medium is shown in figure 3.6. This example shows that during high extraction the center part of the Gaussian input laser beam extracts the energy faster than the surrounding area. This leads to saturation for the central part of the beam faster than the outer region and the intensity starts to drop in the central part due to the loss from each pass. However, the region around the center still continues to amplify as it goes through a region with gain. The result is an increase in beam size at first and if the beam passes through the amplifier, the beam shape changes to a ring which grows in radius with time. Therefore, even if the pump and the laser spots are matched we can never get 100% extraction efficiency from an amplifier. This model is helpful to calculate the expected extraction efficiency and to determine the maximum number of passes the amplifier should be designed for. It is important to mention that the Fresnel diffraction effect is not considered in this calculation. Such diffraction will cause the high intensity regions to diverge in space and time which in turn would lead to smoothing of the features shown. This calculation shows the dynamic effect of the changing distribution of population inversion in the gain medium.

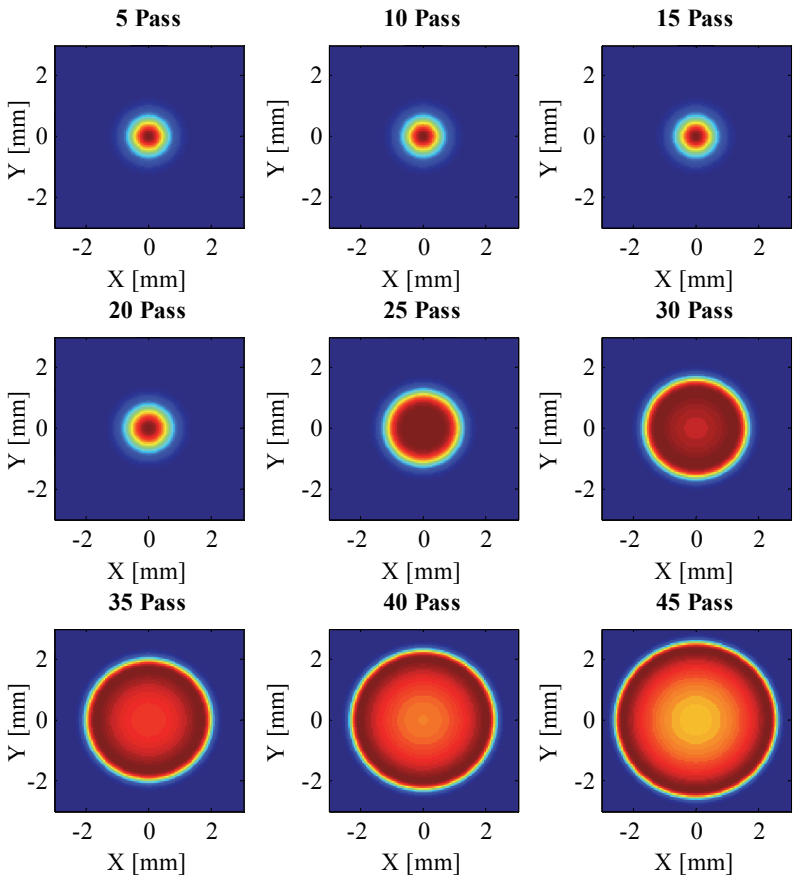

Figure 3.6: Beam fluence distribution measured in J/cm^2 is plotted to show the evolution of beam size at high extraction where a 10 at. % doped Yb:YAG is pumped at 25 kJ/cm^2 and energy is extracted with a Gaussian shaped seed beam with peak fluence of 10 μJ/cm^2. A cavity loss of 5% per pass is assumed for the simulation.

If the parameters are set correctly this model can calculate the performance of a regenerative amplifier with good accuracy where the pump and laser beam both are perpendicular to the crystal or a multipass amplifier where the incident angles of the laser beams are very small with good overlap with the pump. The incident angle usually becomes larger for multipass amplifiers and often the overlap of the pump and the laser beam becomes worse. To calculate the output of multipass amplifier correctly we need a full three dimensional finite element model that can

take into account the geometric alignment too. We have designed our initial multipass amplifier with very small angles. Hence, this matlab model which assumes coaxial beams can predict the output with good success. Nevertheless, we have also developed a three dimensional model using Comsol Multiphysics 4.3 using the high speed computing cluster provided by the nanoFAB facility of University of Alberta for accurate modeling. The model is explained in section 3.4. Before giving details of the Comsol model, we have first verified our matlab model with the some experimental measurements reported in literature at room temperature and also at cryogenic temperature as described in section 3.3.2 and 3.3.3.

3.3.2 Model Verification at Room Temperature

As a first test we have simulated the regenerative amplifier described in reference [37] at room temperature. The layout diagram is shown in figure 3.7 and the simulation parameters are summarized in table 3.3.

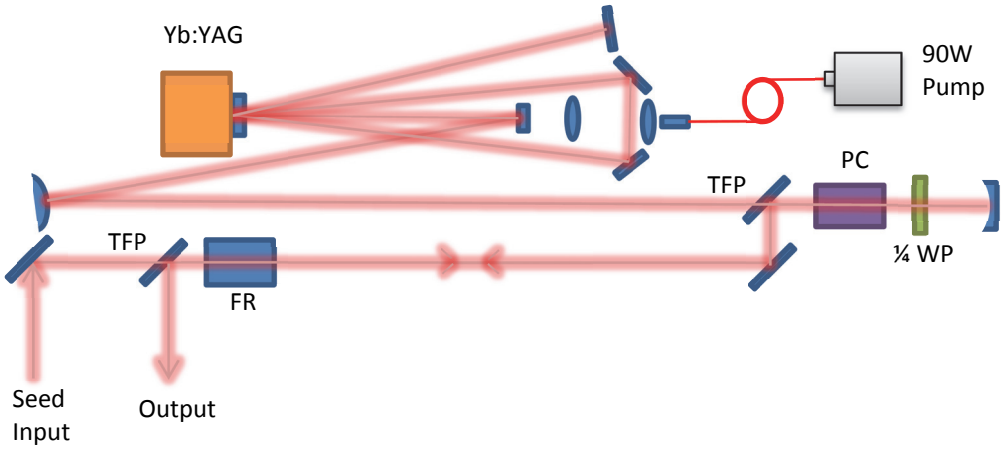

Figure 3.7: Schematic diagram of the system used in [37]. (TFP: Thin Film Polarizer, FR: Faraday Rotator, WP: Waveplate, PC: Pockel Cell)

Table 3.3: Parameters for the system described in reference [37]

Crystal Parameters:	
Length of the Crystal	1 mm
Doping	10%
Pumping Conditions:	
Pump Power	86.5 Watts
Pump Pulse Width (square pulse)	2 ms
Pump Beam Diameter (Flat top)	700 μm
Seed Pulse Energy	20 nJ
Seed Beam Diameter (FWHM,Gaussian)	320 μm
Passive Loss per Pass used	5%

They have measured a peak pulse energy output of 3.4 mJ after 2 roundtrips of the full cavity (16 single-direction passes through the amplifier medium). It is important to mention that that the authors have not mentioned the total losses in the cavity explicitly. However, the losses can be estimate from their cavity layout shown in figure 3.7 by estimating the losses in different components. After 16 passes, the beam crosses a Faraday rotator twice, a thin film polarizer 8 times, a pockel cell 6 times, a quarter waveplate 6 times, and goes through 32 reflections from mirror surfaces. From this information the losses in the cavity may be estimated. The crystal absorption at 1030 nm is automatically considered in the model. By considering a 5% loss in pockel cell and 1% in the other optics, we get a combined loss of ~55% after 16 passes. Therefore we think a loss of 5% per pass is a reasonable assumption for the simulation. For this system our model predicts a peak output of 3.9 mJ after 17 passes with an output energy of 3.6 mJ after 16 passes as shown in figure 3.8. It is also a reasonable to assume an additional 5% loss during switching the pulse out of the cavity. Therefore, the

expected pulse energy is ~3.4 mJ from the output of the regenerative amplifier. Considering the complexity of the system our model prediction and their measurements are in very good agreement.

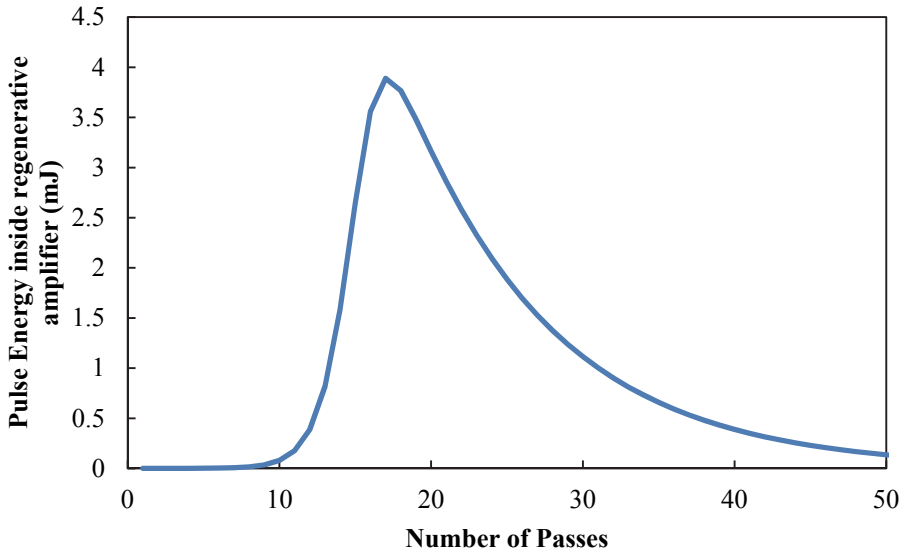

Figure 3.8: Output pulse energy versus number of round trip passes for the simulation of the system parameters reported in [37] at room temperature

3.3.3 Model Verification at Cryogenic Temperature

As the absorption and emission cross-sections are highly temperature dependent it is important to explore a cryogenic amplifier in order to build a compact system with higher gain. Therefore, we have compared our model prediction with the system performance of the Colorado State University group as reported in references [3,70]. The layout diagram is shown in figure 3.9 and the system parameters are summarized in

table 3.4. The laser pulse goes through 8 mirror reflection and twice through a thin film polarizer, twice through a quarter waveplate and twice through a pockel cell

per double pass through the crystal. Assuming a 5% loss in the pockel cell and 1% in other optics, we get a combine loss of 15% per double pass or 7% per single pass.

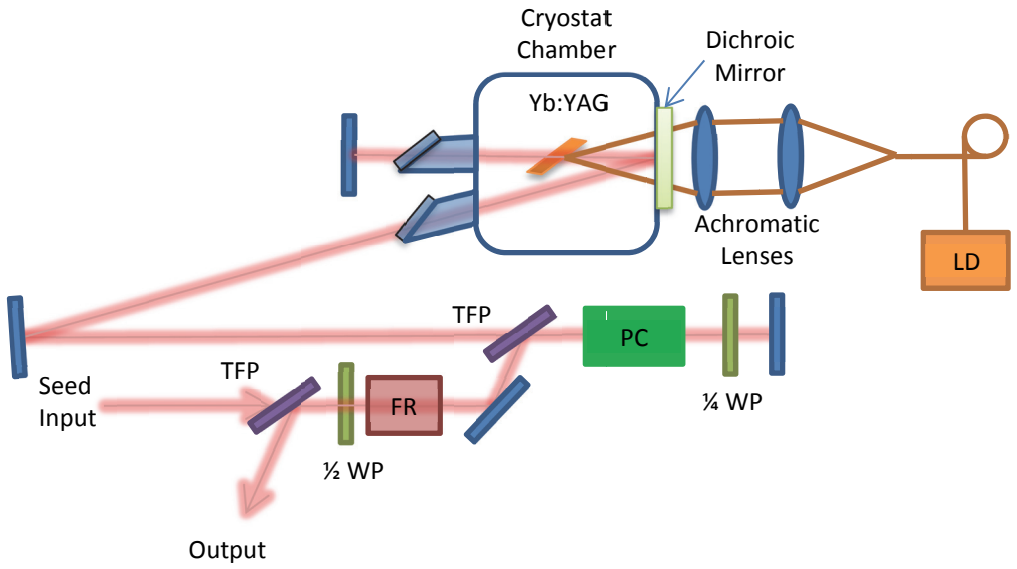

Figure 3.9: Layout diagram of cryogenic regenerative amplifier used in [3,70]. (TFP: Thin Film Polarizer, FR: Faraday Rotator, WP: Waveplate, PC: Pockel Cell, LD: Laser Diode)

Table 3.4: Parameters for the system used in reference [3]

Crystal Parameters:	
Length of the Crystal	2 mm
Doping	5%
Crystal Temperature	100 K
Pumping Conditions	
Pump Power	90 Watts
Pump Pulse Width (square pulse)	1.2 ms
Pump Beam Diameter (Flat top)	700 µm
Seed pulse energy	20 nJ

Seed beam diameter (FWHM, Gaussian)	560 µm

For this system the authors have measured a peak pulse output energy of 7 mJ. They have not reported about the number of passes required to achieve this energy. Our model predicts a peak pulse energy of 7.3 mJ after 10 passes. If we assume an addition 5% loss during the swithing out, the expected output from the regenerative amplifier would be ~6.9 mJ. Again the simulation results are in good agreement with the reported measured output.

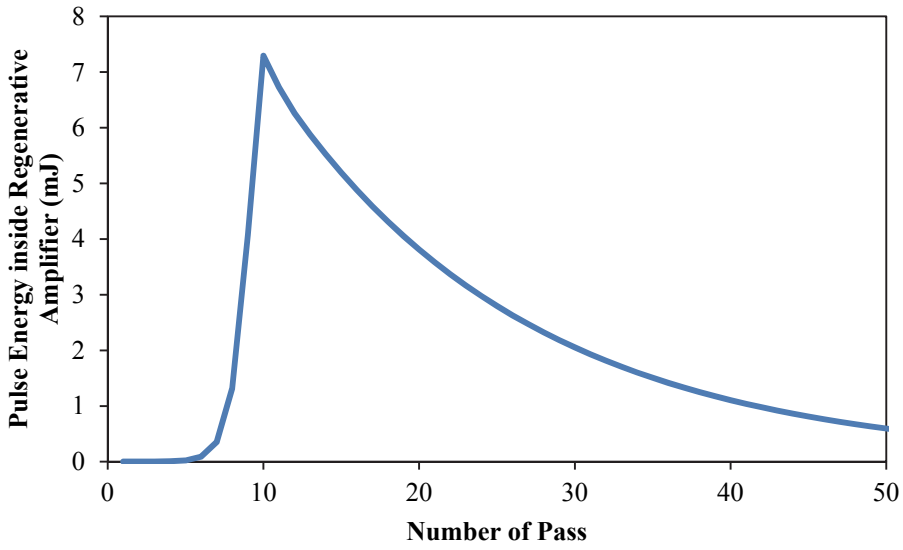

Figure 3.10: Simulation result for the system parameters reported in [37] measured at 100K

From the above comparison, we can say that our model can be expected to predict the operating point of the amplifier successfully. However, these calculations are assuming that the direction of the pump and the laser beam is perpendicular to the laser crystal which is not the case for a multipass amplifier. In the multipass amplifier the laser beam is always coming at some angle and for each pass the

angle could be different. It introduces two problems. The first problem is that when the beam is coming at angle, it changes the gain length. The second problem is when there is significant extraction of energy, the beam will also become distorted after each pass due to the inhomogeneous distribution of the stored energy within the crystal. Therefore, to model the amplifier under high energy extraction conditions it will be beneficial to use a three dimensional model instead of a two dimensional model.

3.4 Three Dimensional Model in Comsol

COMSOL Multiphysics software is a powerful simulation program to solve problems involving systems of partial differential equations (PDEs) using finite element (FEM) techniques. It has different add-on modules such as AC/DC, Acoustics, Heat Transfer, MEMS, RF, PDE etc. COMSOL allows combining multiple modules together sharing the same parameters and to produce more realistic results. The heat transfer and multiple time-dependent PDE modules are used together to model the amplifier in this thesis.

3.4.1 Description of the Model

A separate time-dependent PDE module is used for each differential equation to get the freedom to adjust the equations and parameters in the simulation at each level. For example, to model the pump absorption, population inversion calculation and single pass of the laser beam through the crystal, three different modules are used instead of solving all the equations in one single module. In addition separate modules are used for modeling each additional pass. This

allowed us to set the boundary conditions for each pass with the necessary adjustment of losses, angle of incidence and the position of the beam on the gain medium. A limitation of this model is that it will lead to a complex system to model very high number of passes through the gain medium. However, the multipass amplifiers are usually designed for few passes. Therefore, it is not very difficult to implement this approach. Modeling in COMSOL involves several steps as explained in the following sections.

3.4.2 Geometry Setup

The first step toward COMSOL modeling was setting up the geometry as shown in figure 3.11. The back surface is the surface of the dichroic mirror to reflect the laser beam and to allow the pump to transmit through. There is a 0.5 mm gap between the gain medium and the dichroic mirror to resemble the gap created by a Teflon sheet with a 9 mm × 9 mm hole to avoid scratching on the surfaces of the optics. The gain medium is 2 mm thick as our Yb:YAG crystal is 2 mm thick. To consider the large pump intensity gradient near the edge of the pump the geometric segmentation is created as shown in figure 3.11 so that COMSOL creates a higher density mesh around the partitions to track the large pump gradient. As explained in section 4.3, the crystal mount is designed to cool the crystal from two adjacent surfaces as shown in figure 3.11.

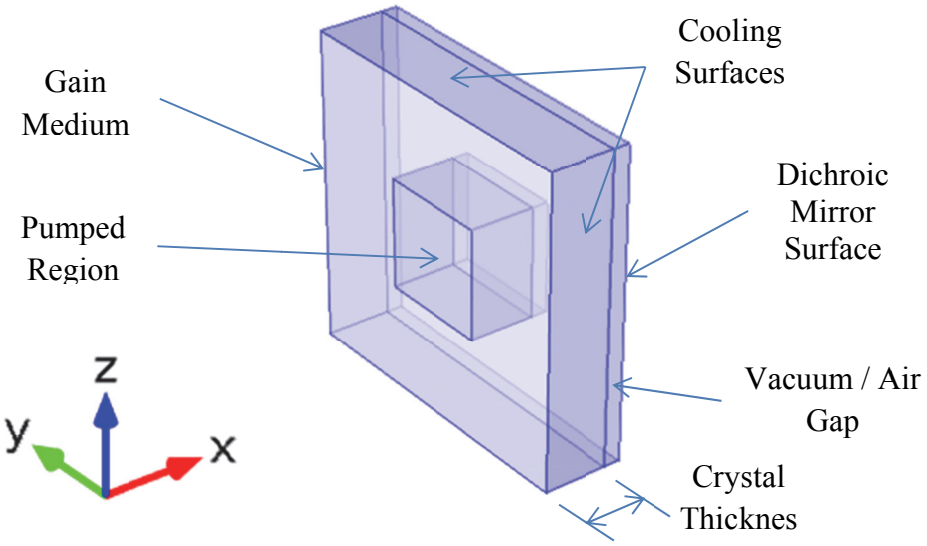

Figure 3.11: Geometry setup in COMSOL

3.4.3 Boundary Condition and Physics Setup

For modeling the pump, a smoothed (10^{th} order supergaussian) top hat pump beam is considered as shown in figure 3.12 given by the following equation,

$$P_{pump} = P_{max} \exp\left(-\frac{x^{10} + y^{10}}{d_P^{10}}\right) \qquad (58)$$

The boundary condition of the pump intensity is applied on the dichroic mirror surface behind the gain medium. Then the material properties of Yb:YAG such as population density, emission and the pump absorption cross-sections, refractive index etc. are defined in the gain medium. Equations (54)-(56) are modeled using two separate PDE modules to calculate the pump absorption and the population inversion. Plots of pump absorption and the population inversion along the XY plane through the center of the gain medium are shown in figure 3.13 and figure 3.14 respectively.

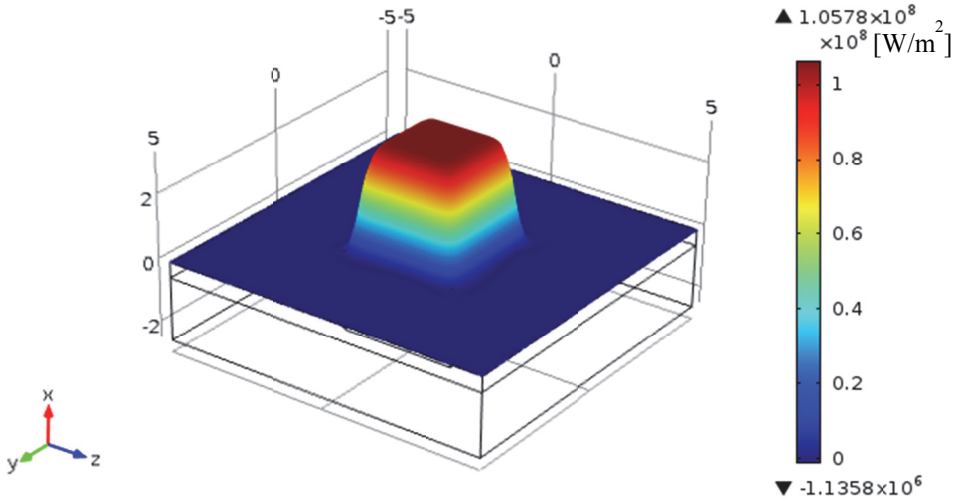

Figure 3.12: Pump intensity distribution when a 3 mm × 3 mm spot of the gain medium is pumped with a total power of 900 W

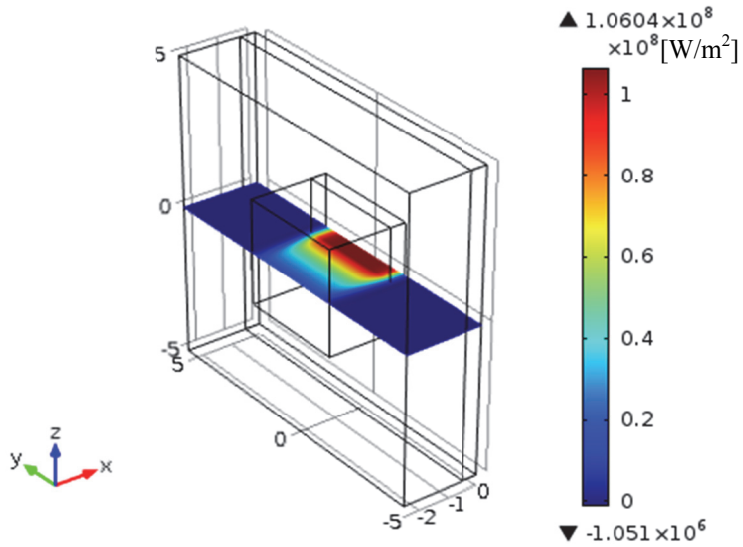

Figure 3.13: Pump absorption in a 3 mm × 3 mm spot inside the crystal along the 2 mm thick gain medium.

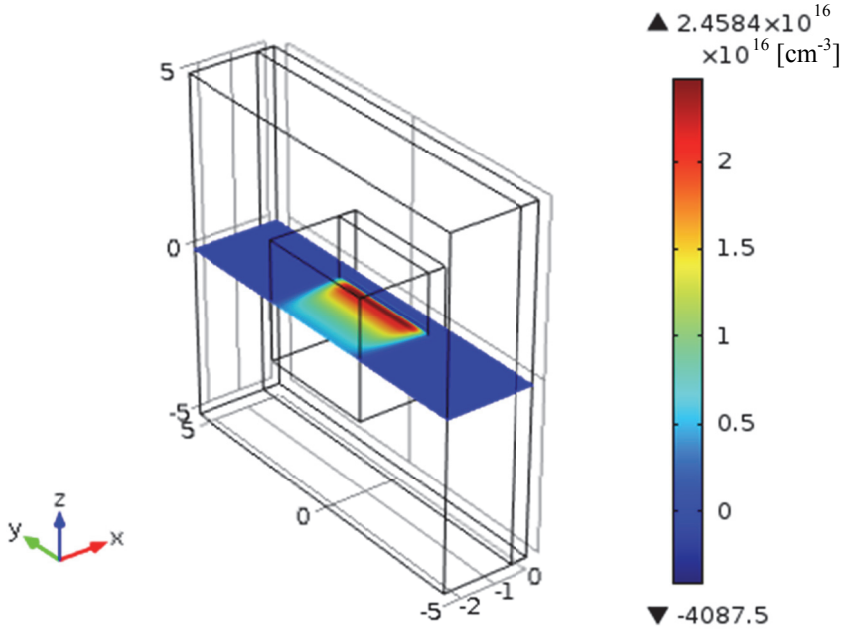

Figure 3.14: Population inversion

The next step is to model the laser beam to calculate the pulse amplification. Since for our experimental measurement we have used a continuous wave (CW) laser as a seed source, our model is designed for a CW laser too. The boundary condition for the incoming laser beam is applied on the front surface of the gain medium and the boundary condition for a reflected beam from a dichroic mirror is applied on the dichroic mirror surface. The pulse amplification is modeled using equation (57). This finite element model can also calculate the amplification of the input laser beam coming at an angle as shown in figure 3.15.

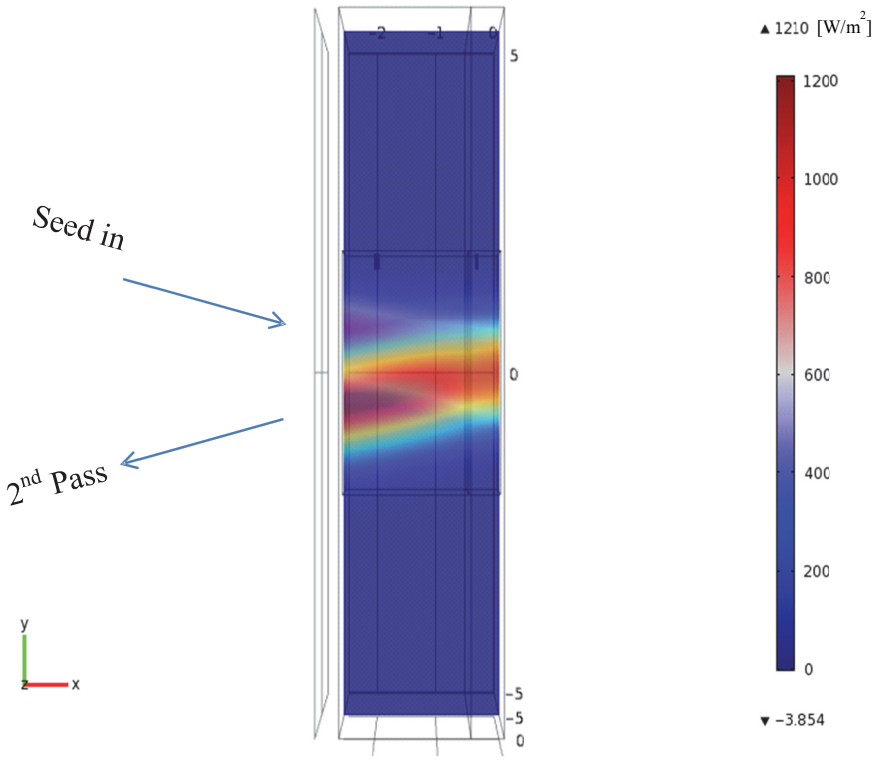

Figure 3.15: Plot of laser pulse energy inside the gain medium

3.4.4 Model Verification

The Comsol model is then then verified by comparing the results with the Matlab calculations. When the pump and the laser optical direction is perpendicular to the crystal surface, both Comsol and matlab should give us the same results. Therefore, we have calculated the pump absorption, population inversion and the pulse amplification in both the simulation platforms and compared. They produce results within 1% of difference. This was done for the cases of double pass gain with variable pump from 0 to 40 J/cm^2 for different temperatures. The results are shown in figure 3.16 where a 10 at. % doped 2 mm thick Yb:YAG was pumped with different pump fluence at several temperatures. A seed with fluence of

1.27 $\mu J/cm^2$ is them amplified in a double pass configuration. The pump and the seed propagation direction is assumed to be perpendicular to the gain medium surface in both cases.

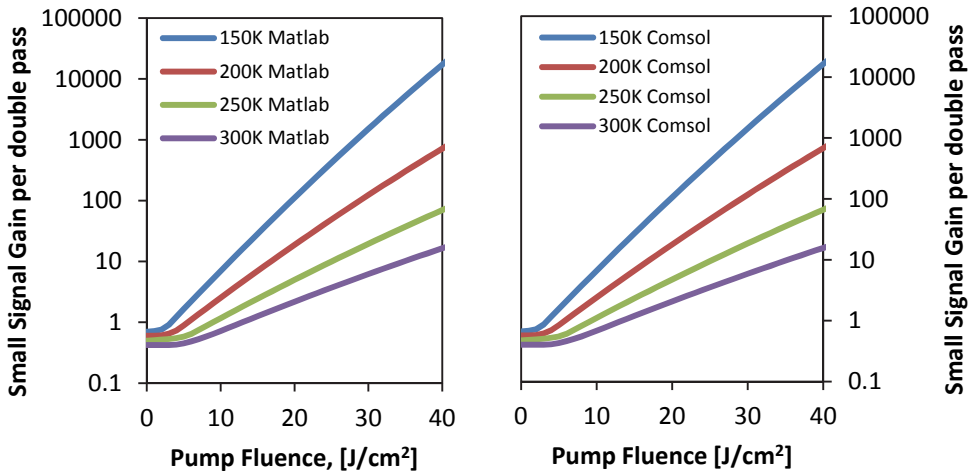

Figure 3.16: Comparison of the double pass gain predicted by Matlab and Comsol model for few test cases. A seed with fluence of 1.27 $\mu J/cm^2$ in 1 ms is amplified as it passes through a 2 mm thick Yb:YAG gain medium at different pump and temperatures.

Chapter 4 Experimental Setups

4.1 Seed Laser

A continuous wave tunable wavelength laser oscillator was built to use as a seed source to measure the gain of the amplifier as shown in figure 4.1. A fiber coupled laser diode generating 9 W at a drive current of 11 amperes was used as a pump source. The output beam of 105 μm diameter was imaged with a 1:1 magnification into the crystal. A Z cavity configuration is used to correct for astigmatism due to the Brewster angled crystal. A prism was included in cavity to give wavelength tuning. The laser crystal used in this oscillator is a 2 at. % 5 mm thick $\mathrm{Yb:CaF_2}$. The Laser Cavity is shown in figure 4.1. The Yb:CaF_2 laser has a fairly broadband output and the laser wavelength can be tuned between 1020 nm to 1060 nm. Since the Yb:YAG has an emission peak at 1030 nm, this laser was tuned to 1030 nm for the gain measurement. The output beam diameter was ~1.5 mm, ($1/e^2$ intensity) at the output mirror. The CW output power measured at 11 A drive current was 1.2 W. Some fluctuations of output power of the order of a few percent at 10 kHz was observed.

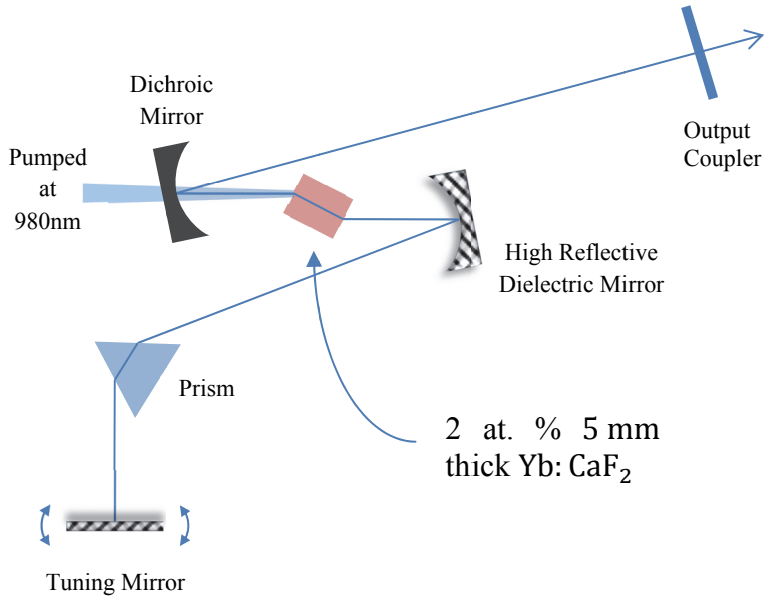

Figure 4.1: Tunable laser oscillator

4.2 Multipass Amplifier

Initially the amplifier parameters were studied at room temperature to verify and quantify the behavior in a regime where the crystal parameters are well known. Then we studied the performance at various cryogenic temperatures using our model. Using the setup shown in figure 4.2 we have measured the pump energy and calibrated an energy monitor calorimeter to measure the pump energy.

Beams from two DILAS diode lasers [71] are combined with a beamcube polarization combiner. Each laser diode can provide a maximum of 2 kW power. The combined beam is then passed through a weak diffuser (LSD holographic diffuser from Luminit with a light shaping diffuser angle of 0.5^0 FWHM) to homogenize the beam. The beam is then focused into the power meter using a 75 mm spherical lens through a calibrated wedge, a dichroic mirror and an ND3

filter. The reflection from the front surface of the wedge is measured to be 4.2% of the incident pump using the power meter at low repetition rate (<8 Hz). The monitor energy calorimeter is used to measure the pump energy real time during the experiments. The dichroic mirror is used so that the 940 nm wavelength component (pump) can pass through and the 1030 nm component (seed) is reflected. This allows the pump and the seed to come from the opposite sides. The ND3 filter is used to reduce the pump intensity to protect the power meter. The ND3 filter is calibrated at 940 nm by measuring the power at low intensity with and without ND3 filter. The transmission at 940 nm wavelength is found to be 0.0023 ± 0.0006. The calibration error of the ND3 filter is high mainly because we have used a low pump repetition rate (8 Hz) that creates fluctuation of the power indicator. Moreover, the reduced light through the ND3 filter is in the lowest range of the power meter which is the least accurate range of the power meter. A Spectra-Physics (407A) calorimeter was used as the main calorimeter and a 4" painted pyroelectric crystal type calorimeter was used as the monitor calorimeter.

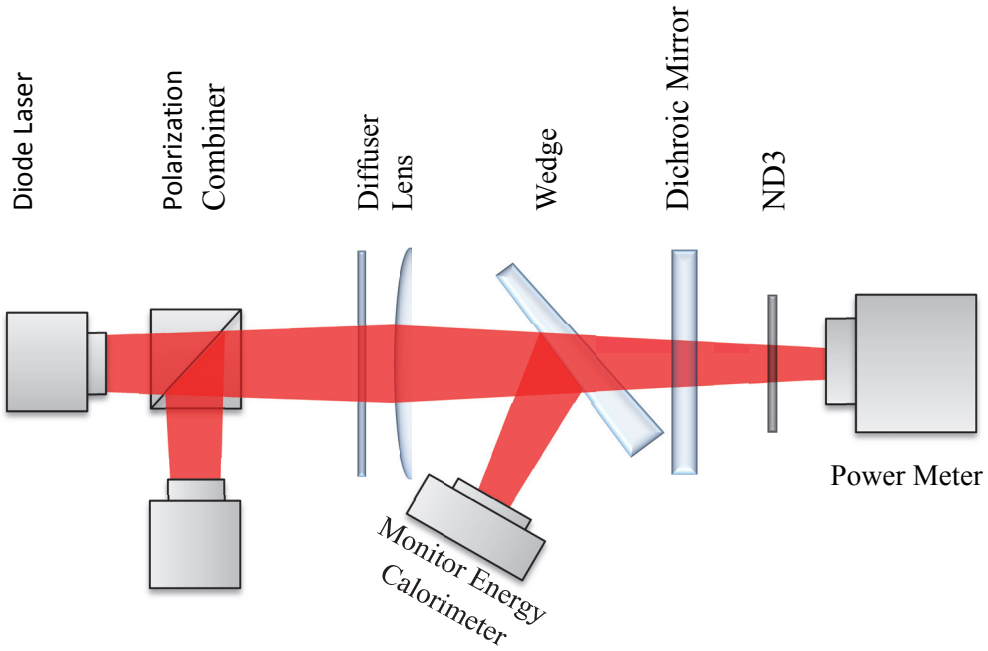

Figure 4.2: Layout of the pump diode configuration and setup used to measure the pump energy and calibrate the monitor energy calorimeter

After calibrating the energy meter, we have measured the absorption of the pump in the crystal using the geometry shown in figure 4.3. To produce a small pump spot we had to use a plano-convex lens of focal length of 7.5 cm and a diameter of 5 cm. Since the pump beam is divergent, we could not place the lens very far away from the laser diode to produce smaller pump spots because we would lose a large amount of the beam energy. Also we could not go very close to the laser diode to capture most of the light energy because the spot size would be so large that the pump intensity would drop at the laser crystal. We found a balance between these two when the lens was 35 cm away from the laser diode with the curved side of the lens facing the pump diode. The input energy is measured using the calibrated energy meter and the transmitted power was measured using the same power meter to calculate the absorbed energy. The total absorption was

calculated from the above measurements and compared with the simulation results. The plots of the data taken are shown in figure 5.3 in Chapter 5.

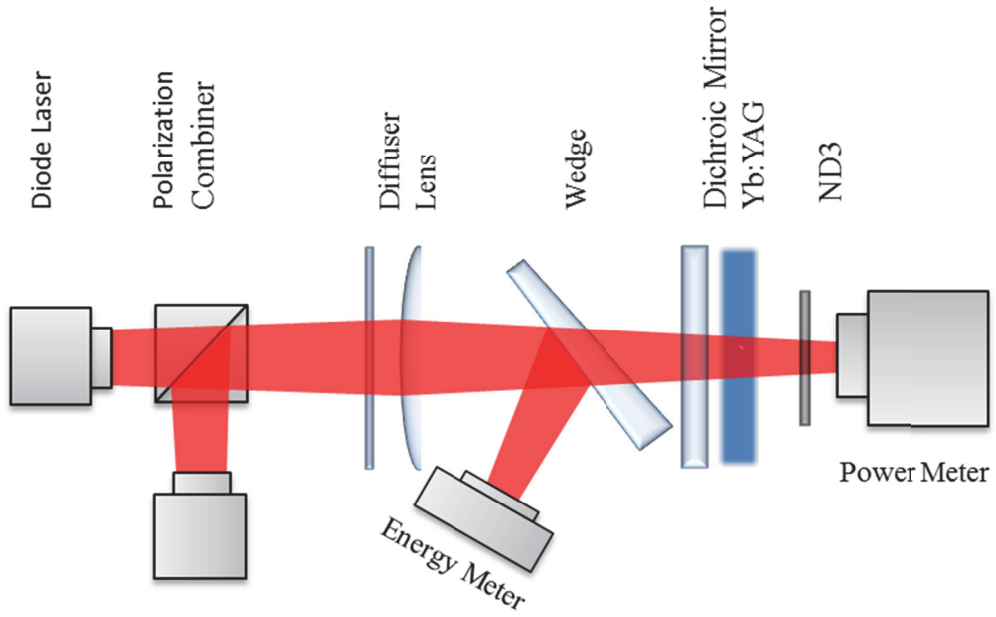

Figure 4.3: Experimental setup used to make the absorption measurement

Finally to measure the gain we have explored two geometries to choose the best approach of building the final stage amplifier. In the first geometry as shown in figure 4.4, we have tried to take the beam into the crystal from the same side so that we can use a simple high reflective mirror behind the crystal. This would allow a double pass of the pump through the crystal that will increase the amount of absorption in the crystal. In the second geometry, the pump and the laser beam were incident from opposite side as shown in figure 4.5.

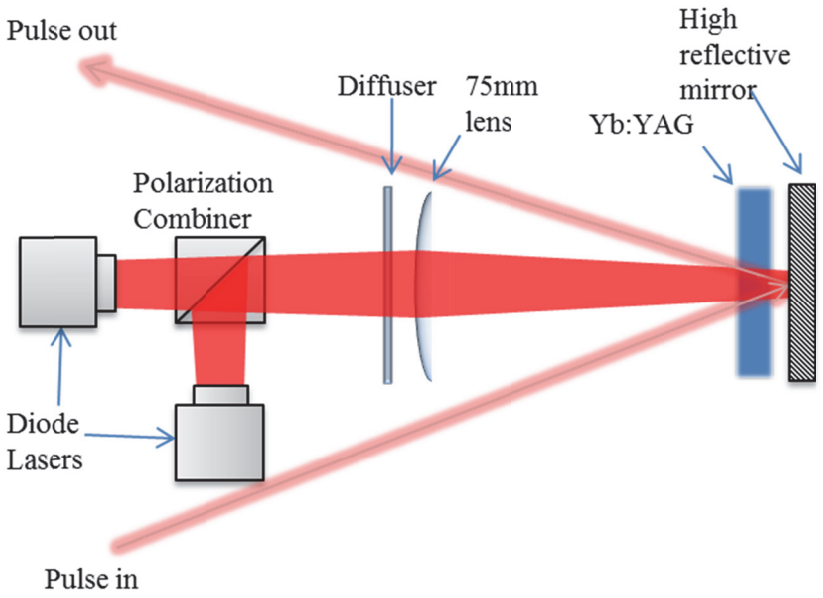

Figure 4.4: Front pumping geometry

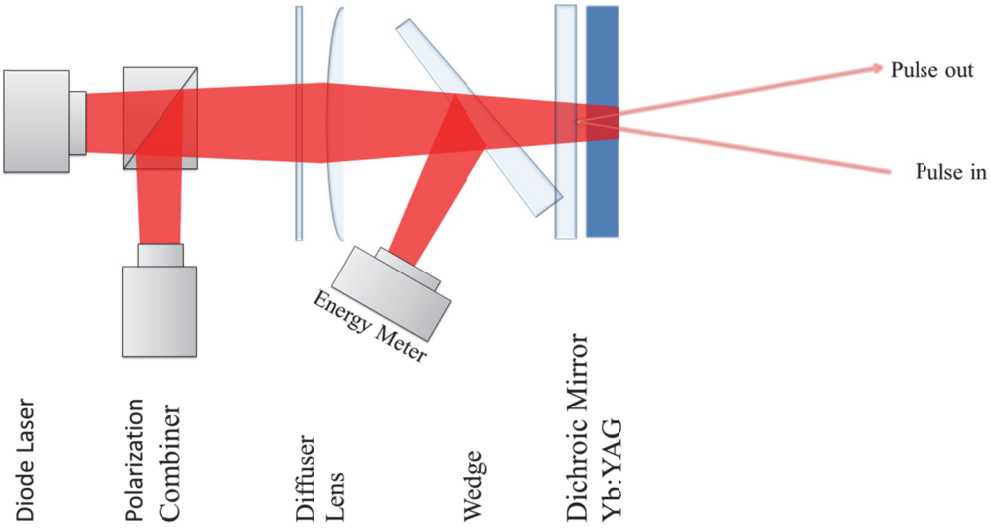

Figure 4.5: Rear pumping geometry

By considering the design and the limitations of a cryogenic system, the geometry shown in figure 4.5 was chosen for our final amplifier tests. In this geometry the crystal was pumped through the dichroic mirror from one side and the input pulse entered from the opposite side of the crystal. Laser beams from two DILAS laser diodes were combined using a polarization combiner. Since the pump diode was composed of many diode strips, the beam was not homogeneously distributed over the pump spot. Therefore, a diffuser was employed to make it more homogeneous and to avoid forming of any hotspots on the crystal. Using a lens of focal length, $f = 7.5\,\text{cm}$ at object and image distance of 35 cm and 9.5 cm respectively, the beam was focused onto the crystal to produce a $2.5\,\text{mm} \times 2.5\,\text{mm}$ spot on the crystal. Moreover, a wedge was used to reflect a small portion of the pump energy to an energy meter to observe the pump energy of each pump pulse. Pumping the crystal from the back allowed us to obtain a good overlap of the pump and seed beam while pumping a small spot. This double pass geometry was used to quantify the amplifier parameters and to study the initial amplifier performance.

A more complex beam four pass geometry as shown in figure 4.6 was then used to measure the multipass gain. In this geometry the seed beam of diameter ~2 mm comes in perpendicular to the crystal plane and focused on the dichroic mirror using a lens of focal length of 50 cm creating a spot size of 0.44 mm (FWHM). If the lens and the dichroic mirror are separated by the focal length of the lens, the reflected beam will be parallel to the incident beam after crossing the lens again. Using two mirrors at 45 degrees and proper alignment, it is possible to have

multiple passes through the gain medium with no additional mirror or component as shown in figure 4.6. A similar geometry was reported in [72]. This geometry allowed us to reimage the beam back into the amplifier after each pass and potentially develop a system with many passes equivalent to a regenerative amplifier. Careful calculation of number of passes needed will facilitate designing a terawatt system purely based on multipass amplifiers without a regenerative amplifier and thus reducing the cost of the system. Unlike conventional multipass amplifier we can increase the number of passes to eight, as shown in figure 4.7, or more with no additional optics.

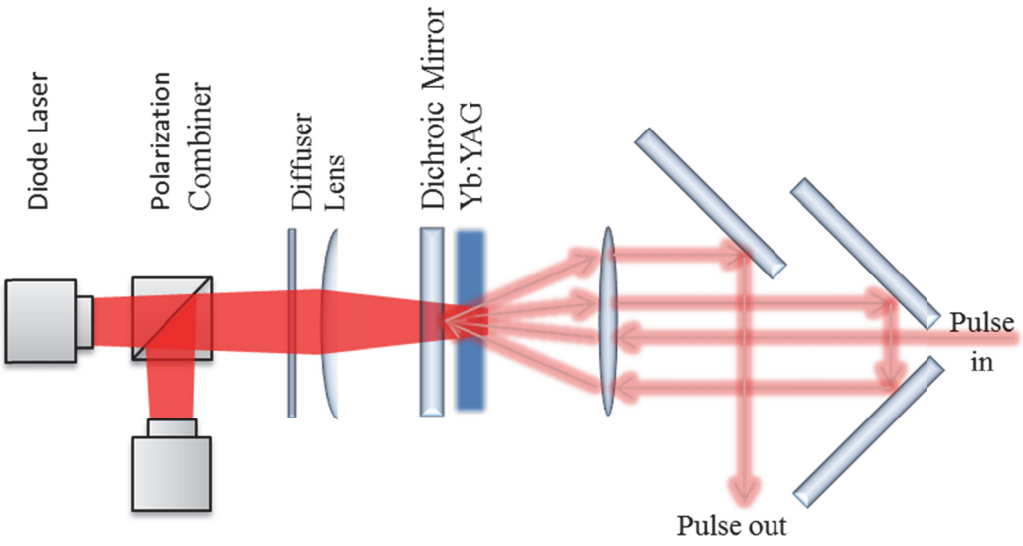

Figure 4.6: A four pass multipass amplifier setup using a lens and three mirrors only

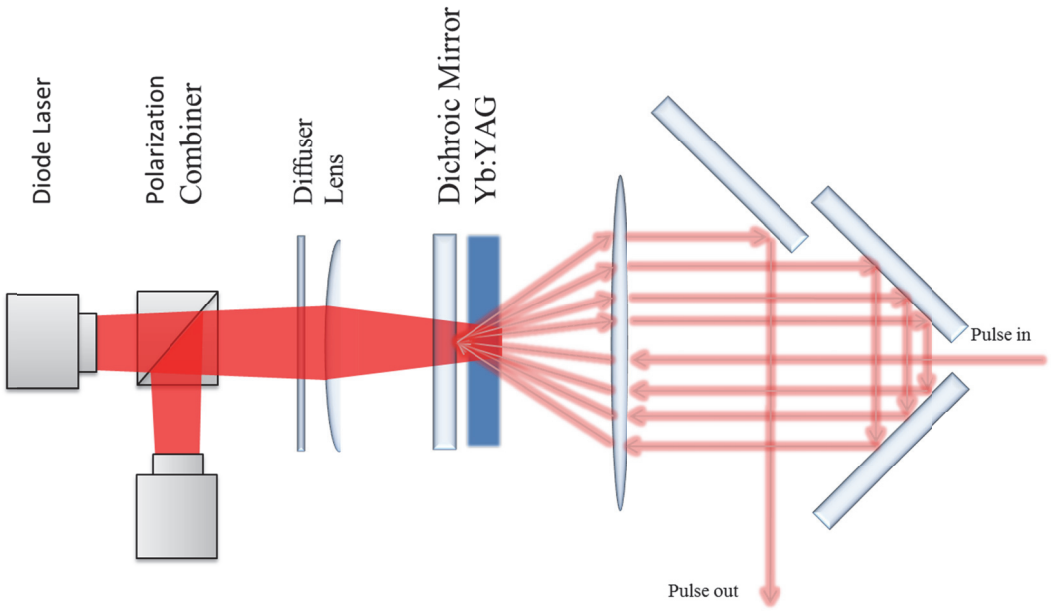

Figure 4.7: An eight pass multipass amplifier setup using a lens and three mirrors only

4.3 Design of Cryogenic System

A cryogenic multi-pass amplifier was designed to be used in the final stage to take the pulse energy to the joule level capable of generating output powers in the terawatt range for picosecond pulse durations. The overall experimental system is shown in figure 4.8 and the cross-section view of the cryogenic chamber is shown in figure 4.9.

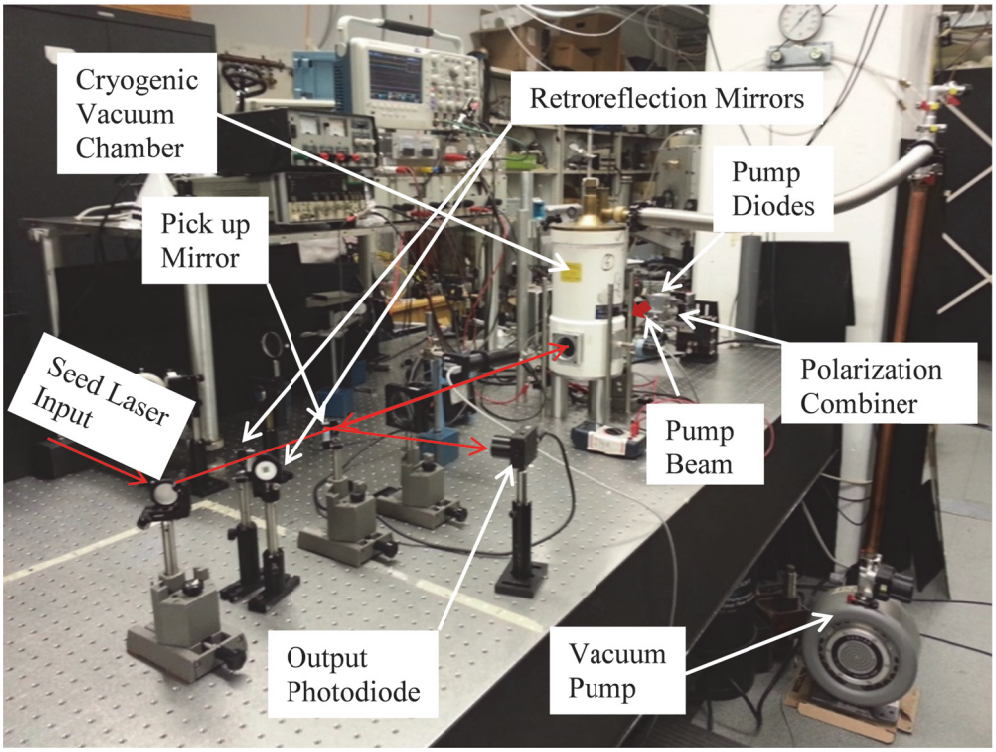

Figure 4.8: Cryogenic multipass amplifier setup

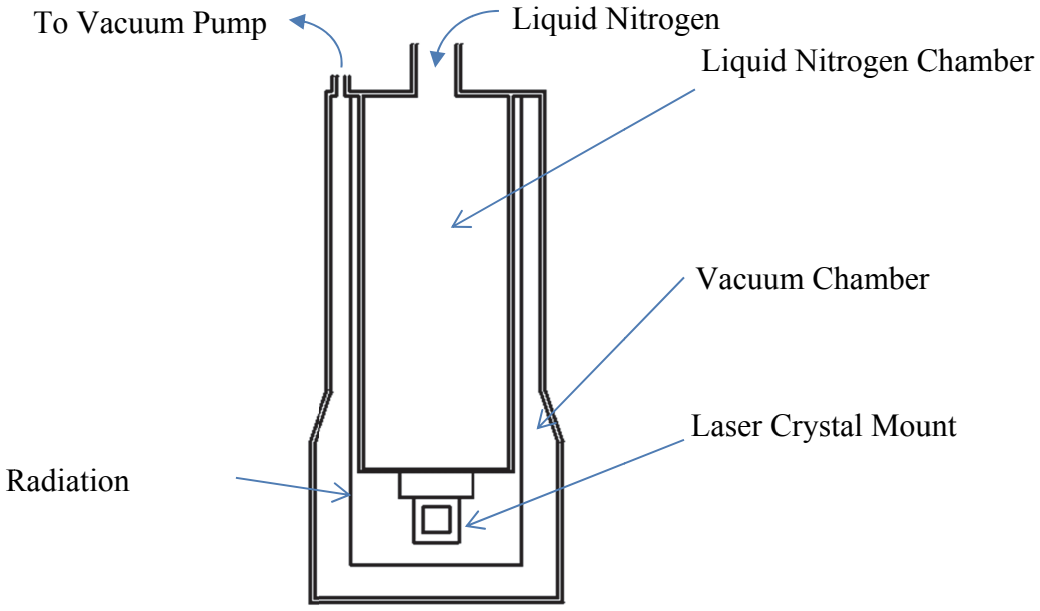

Figure 4.9: Cross-section of the cryogenic system

A 10 mm × 10 mm × 2 mm 9.8 at. % Yb:YAG ceramic crystal was used as a gain medium for the amplifier. The crystal was installed in a custom made Copper mount shown in figure 4.10. The round base of the mount was connected to the bottom of a Copper Cylinder filled with liquid nitrogen and the whole mount was hung upside down carrying the Laser Crystal and the Dichroic Mirror. The cooling of the crystal was done through two nearby edges of the crystal. The dichroic Mirror pushed the crystal against the mount. A 0.5 mm Teflon sheet was used between the dichroic mirror and the crystal to avoid any direct physical contact between them to remove the possibility of scratching the crystal or the mirror. Indium foil was used between the mount and the edge of the crystal to insure the thermal contact between them and to protect the crystal from getting scratched. Two chassis mount resistors of 100 Ω are used to vary the crystal temperature by resistive heating. Four brass washer were used between the liquid nitrogen cylinder and the mount to limit the cooling rate so that the resistors can actually create a temperature gradient in the mount resulting a change in temperature in the crystal. Two chasis mount resistors (RP60515R0100JNBK) from Digi-Key were used to heat the mount for temperature tuning as shown in figure 4.10. Two platinum resistor temperature detectors (PPG102C1) also from Digi-Key were installed in two places of the mount as indicated in figure 4.10 as temperature sensors. The copper mount was attached to the bottom of the cryo cylinder using 4-40 brass mounting screws as shown in figure 4.9. A brass washer is used with each screw to limit the cooling area to the screw and washers. The mount is then placed in a vacuum chamber to thermally isolate the system from

the surrounding. A radiation shield is also used around the mount to prevent heat from escaping through thermal radiation. An important issue is the thermal deformation of the mount that will cause scratching or cracking of the crystal. Since the thermal expansion coefficients are not the same for the crystal and the copper mount, a soft indium foil is used between them to avoid scratching or cracking of the crystal. Again, the liquid nitrogen cylinder and the mount both are made of copper. Therefore, mismatch of the thermal expansion coefficient is not an issue.

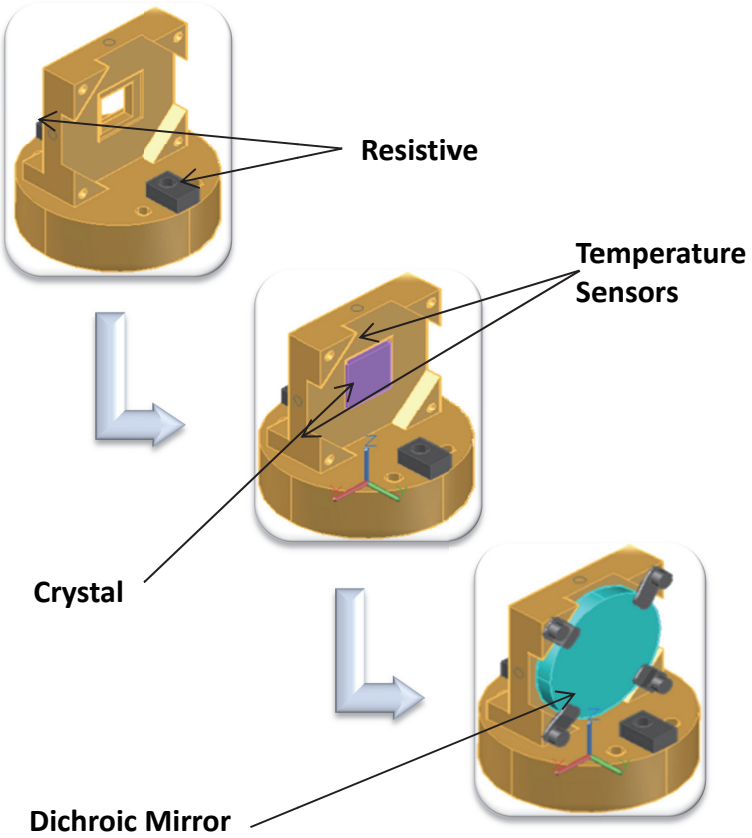

Figure 4.10: Customized copper mount designed for the crystal

Chapter 5 Results and Discussion

5.1 Characterization of Pump

We began our measurement by characterizing the pump beam. The pump spot size on the Yb:YAG crystal was measured by imaging the pump spot onto a CCD camera with a simple positive lens. The CCD camera (Chameleon Camera, Point Grey, Richmond Canada) image is shown in figure 5.1. We have used imageJ software developed by National Institutes of Health (NIH), Bethesda, Maryland, USA for the image processing.

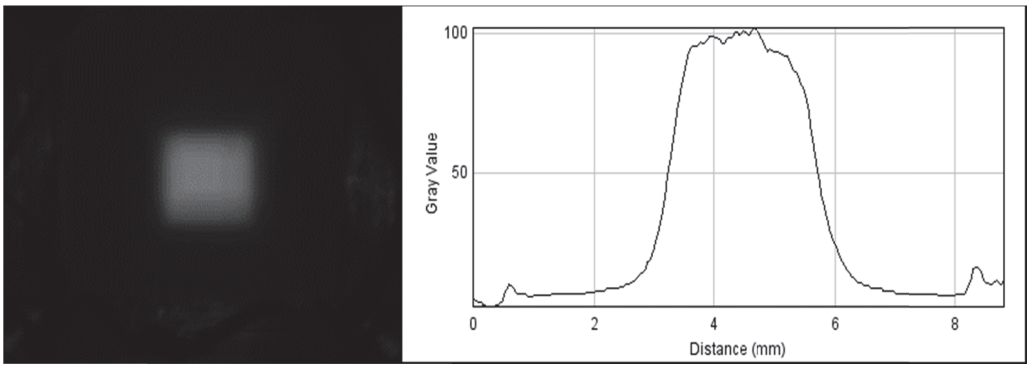

Figure 5.1: Pump spot on the crystal

The output wavelength of the pump diode was measured using an ocean optics USB 2000+ spectrometer with a fiber optic input cable of core diameter of 600 μm and an entrance slit of 25 um. The spectrometer had a spectral range of 520 nm to 1160 nm. The spectrometer was calibrated using a Hg spectral lamp and the calibration accuracy was found to be within 0.6 nm and the linewidth resolution to be of the order of 1.5 nm. We have measured shorter wavelengths than the

datasheet (940.3 nm). The plots in figure 5.2 also show that the wavelength shifts toward longer wavelength with the increasing current and the pulse duration. The reason for this is the temperature dependence of the diode pump lasers that shifts the output to longer wavelength. It appears that the output wavelength would match with the wavelength of 940.3 nm specified on the datasheet if we measure the wavelength in continuous wave (CW) mode. This shorter wavelength reduces the absorption of pump in the crystal since it does not match as well with the absorption peak of Yb:YAG at 940 nm. However, it still absorbs sufficiently that it can give us sufficient gain to build an amplifier. It would also be possible to increase the amount of absorption by temperature tuning the pump diode laser by adding heat to it.

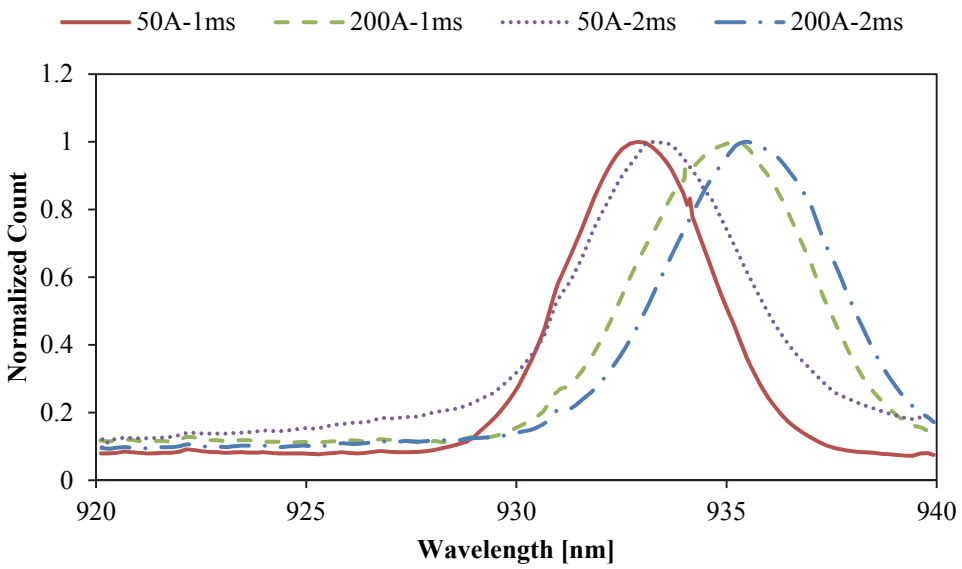

Figure 5.2: Pump spectrum obtained for different current and pulse width combination measured in single shot mode

5.2 Pump Absorption

After spectral measurements we have calibrated the energy meter to observe the pump energy using the experimental setup shown in figure 4.3. The energy meter calibration plot is shown in figure 5.3. The linear calibration plot also allows us to calculate the incident pump pulse energy using a simple linear equation. The absorbed energy in the crystal is then calculated from the incident and transmitted pulse energies in the experimental setup shown in figure 4.3 using equation 1. The measured absorption values are then compared with the simulation using the Comsol FEA calculation in figure 5.4.

$$\text{Absorbed Power} = \frac{\text{Incident Power} - \text{Transmitted Power}}{\text{Incident Power}} \qquad (1)$$

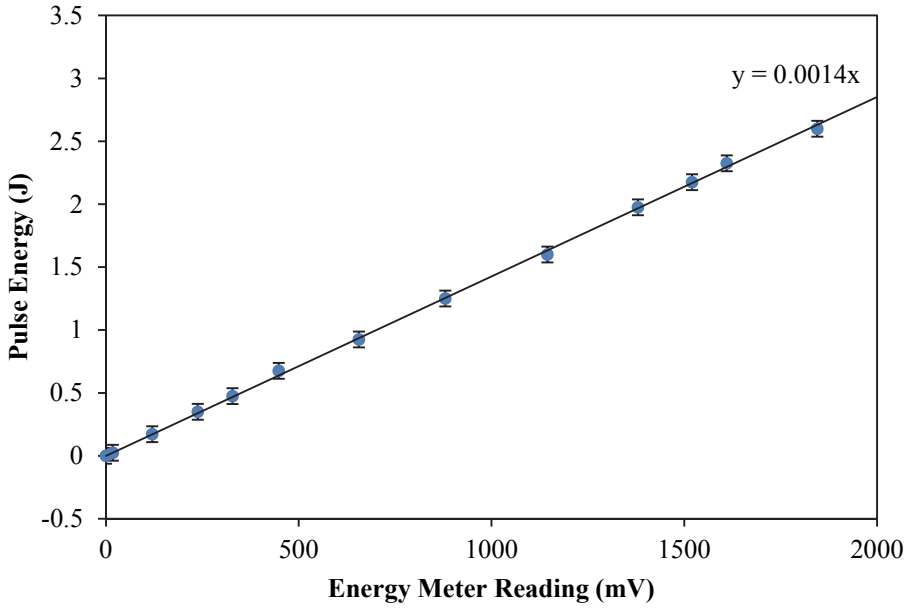

Figure 5.3: Calibration plot for the energy meter

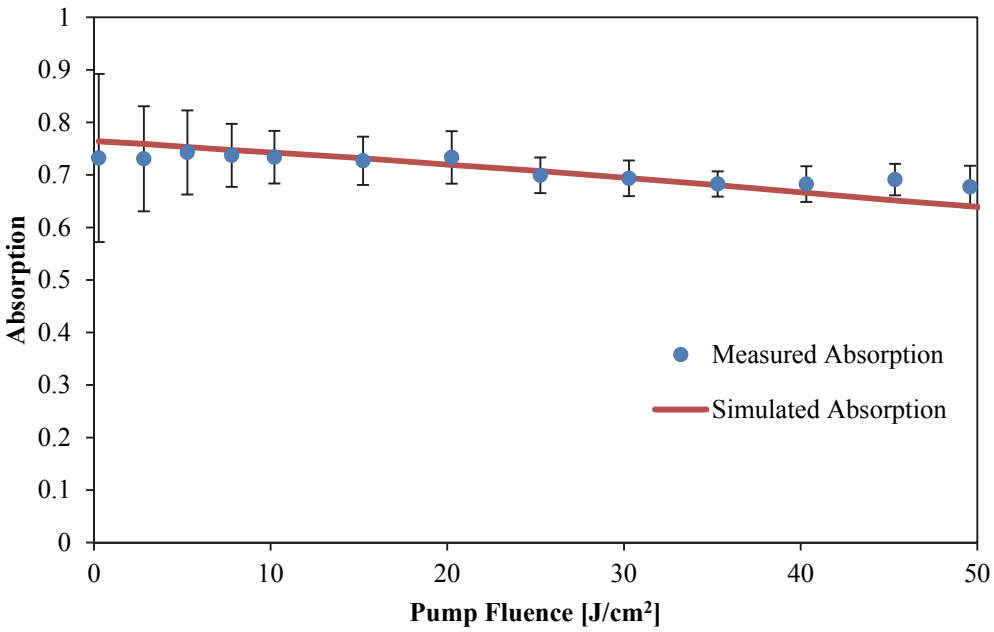

Figure 5.4: Measured and simulated pump absorption

The measured absorptions are in quite good agreement with the simulation up to pump fluence of $35\ \mathrm{J/cm^2}$. Above that, the absorption rate increases. Most likely at such high pump fluence, the wavelength shift may be leading to slightly higher absorption due to the increased absorption cross-section. There could be also a small effect due to increased ASE which depopulates the upper laser level and repopulates the lower level.

5.3 Fluorescence Measurement

To examine whether the ASE is actually a factor we have measured the fluorescence spectrum in the transverse direction and longitudinal direction. If ASE is significant then the spectrum around the emission peak should start to become narrower. According to figure 5.6, up to $35\ \mathrm{J/cm^2}$ the spectrum is narrowed only very slightly but starts to narrow down more rapidly above $35\ \mathrm{J/}$

cm^2. Observation of a small amount of ASE at room temperature is an indication that we might observe more significant ASE problems at cryogenic temperatures as the absorption cross section is very small around 1030 nm at cryogenic temperatures and the emission cross section becomes much higher.

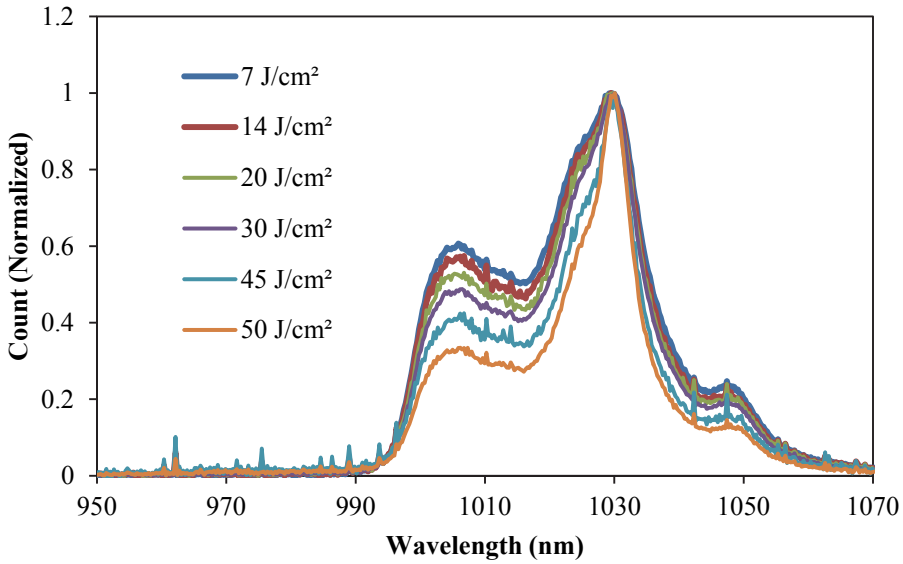

Figure 5.5: Spectra of transverse fluorescence at different pump fluence

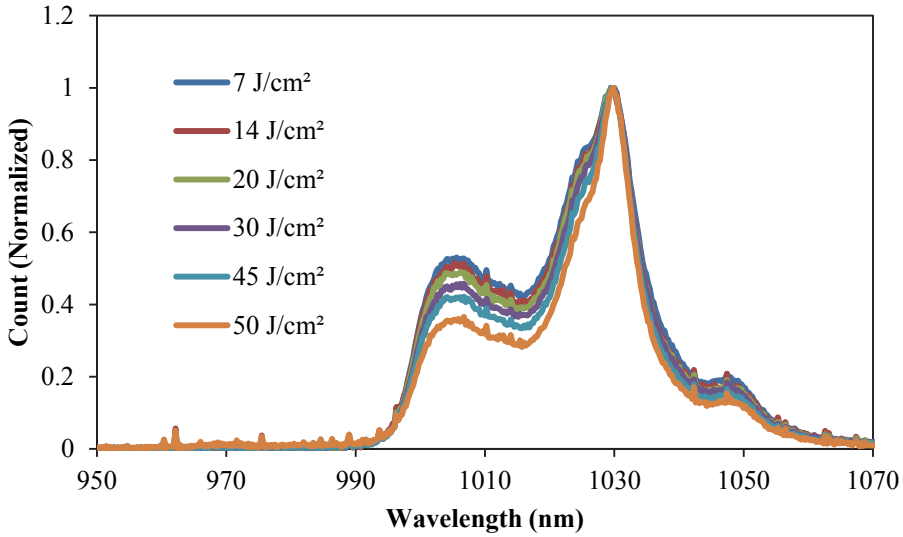

Figure 5.6: Spectra of longitudinal fluorescence at different pump fluences

After characterizing the absorption of the pump laser in the crystal, we have characterized the seed beam. A tunable oscillator shown in figure 4.1 was tuned to 1030 nm and used as the seed laser. The laser output was measured to be 1.1 mW and the beam diameter was measured to be approximately 4 mm (FWHM). The beam is then passed through a 2 mm aperture and focused onto the Yb:YAG crystal using a 50 cm positive lens. The spot size on the crystal measured to be 0.44 mm (FWHM) in diameter as shown in figure 5.7.

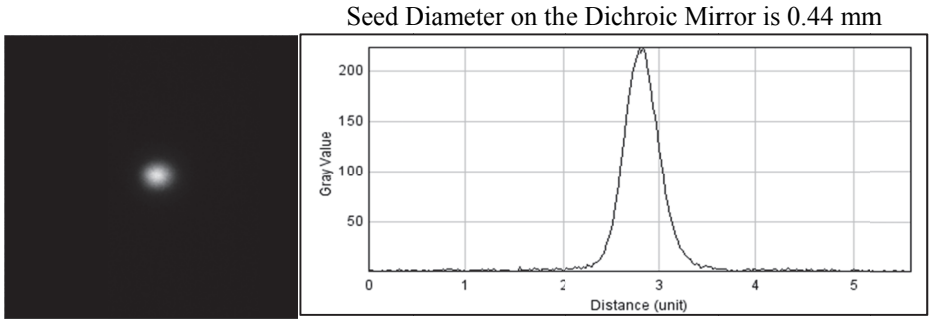

Figure 5.7: Laser spot on the crystal

5.4 Gain Measurement at Room Temperature

First of all the Yb:YAG crystal was imaged onto a CCD camera (Chameleon) to observe the pump and laser spot on the crystal using a 100 mm lens. During the spot size measurement the pump intensity is kept very low to avoid damaging of the camera. The pump diode trigger pulse is used to synchronize the camera. The pump and the laser beam overlap were confirmed using the CCD camera before taking the actual gain measurements. The laser beam passed twice through the crystal because of the back mirror used to reflect the laser beam back through the crystal again. This reflected beam was then taken into a Photo Diode to measure the increase in signal.

To calculate the net gain of the system accurately it is important to consider all the losses. Since we are using an active mirror configuration for our amplifier, we have measured the double pass absorption of the 1030 nm seed beam. First we have removed the crystal from the system and measured the power reflected from the dichroic mirror of 1.1 mW for the incident input seed beam using a power meter. Then the AR coated Yb:YAG ceramic crystal is placed before the dichroic mirror and the signal power was reduced to ~0.44 mW. This gives a double pass transmission of 0.4 ± 0.02 . The calculated transmission using the absorption cross-section of Yb:YAG is 0.41. The difference could be due to the quality of the AR coating or slightly incorrect value of absorption cross section used in the calculation. For a double pass configuration, the beam goes through a reflection from the dichroic mirror, a pickup mirror, and a 50 cm lens. The combined loss of 6% was measured by measuring the power before entering and after leaving the amplifier components. After installing the cryogenic chamber, the loss from the cryogenic entrance window was added into the system and the combined loss of 8.7% is measured per double pass.

Two kinds of pumping geometries as shown in figure 4.4 and figure 4.5 were explored to choose the better one as our final amplifier geometry. The gains measured in both the geometries are compared in figure 5.8. The gain in this case is defined relative to a 100% reflected beam with Fresnel losses for double pass through the crystal taken into account. Thus at low pump fluence the net gain is less than unity due to the absorption in the laser crystal.

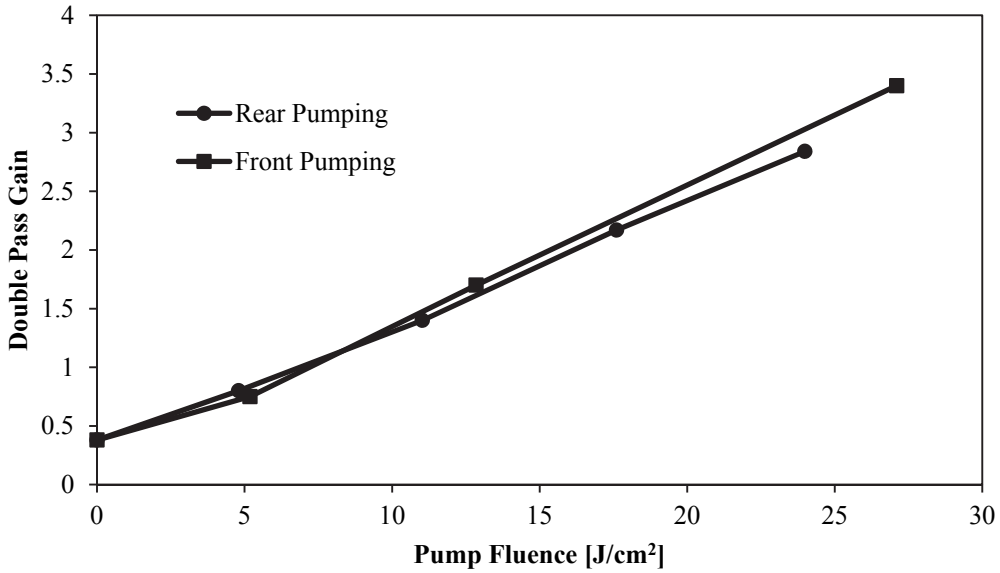

Figure 5.8: Comparison of front and rear pumping geometries

Although the front pumping geometry seems to provide a little bit more gain, the actual difference in gain is not very significant. We obtain more gain in the front pumping geometry because the pump passes twice through the crystal that increases the absorption of the pump to provide more gain. However, since the single pass absorption of the pump is quite strong the extra pumping from the double pass geometry is small and the difference in gain measured is not very large. In addition the angle of incidence of the input pulse is significant ($\theta_{inc} = 23^0$) because of the large solid angle occupied by the pump beam optics. Our goal was to make the system cryogenic so that we could achieve very large gain with a low number of passes through the crystal. The front pumping geometry would require a very large solid angle and entrance window in the cryogenic vacuum chamber to allow all the beams to enter which in turn would increase the heat loss in the form of thermal radiation.

On the other hand the rear pumping geometry provides several other advantages that made this geometry attractive to us although it allows only single pass of the pump beam. First of all, we can keep the angle between the incident and the reflected beam really small that gives very high pump and the laser beam overlap. We can easily install additional measuring instruments such as energy meter to observe the real time pump energy. Finally, we can design beam arrangements to have many passes almost on axis as shown in figure 4.6. Thus we chose the backside pump geometry for our final amplifier. Measured double pass gains for different pump fluences are plotted in figure 5.10. In this case the seed beam diameter (FWHM) varies from 225 µm to 222 µm under linear raytracing assumption and almost remain unchanged under Gaussian approximation as illustrated in figure 5.9.

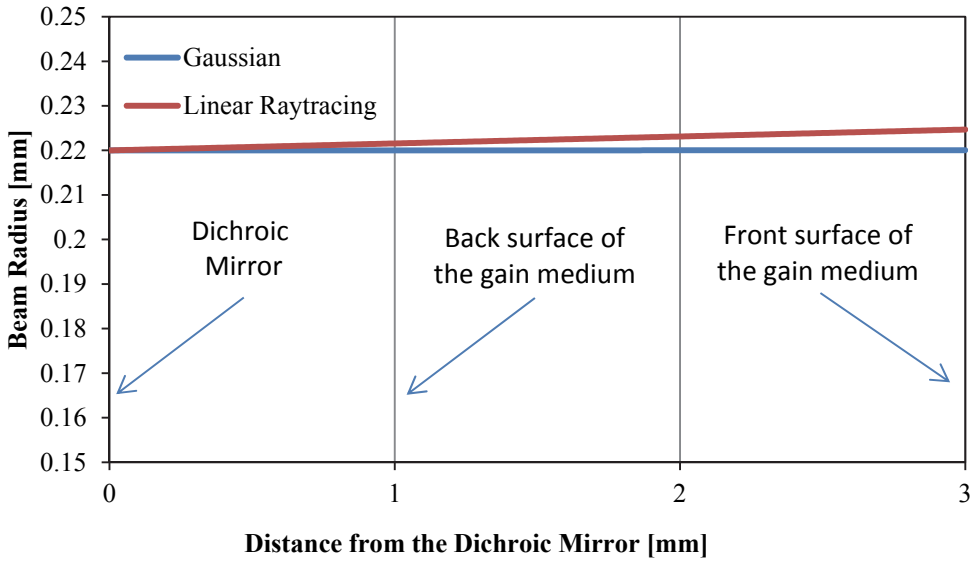

Figure 5.9: Variation of beam radius inside the gain medium

In the next step we employed 8 passes of the laser beam through the amplifier using the geometry shown in figure 4.7. The measured 2 pass and 8 pass gains are then compared with our 3D Comsol FEA model calculations as shown in figure 5.10. The measured gain seems to agree with the simulation at room temperature. In particular we see a saturation in the gain at a large pump fluence of around $30\ \mathrm{J/cm^2}$. This can be understood if one considers the saturation fluence of ~8 J/cm^2 (the absorption cross-section at 1030 nm is also considered) and the fact that the effective amplified fluence of the pulse is ~6 J/cm^2 for the last pass of the 8 pass case indicating significant extraction of the stored energy.

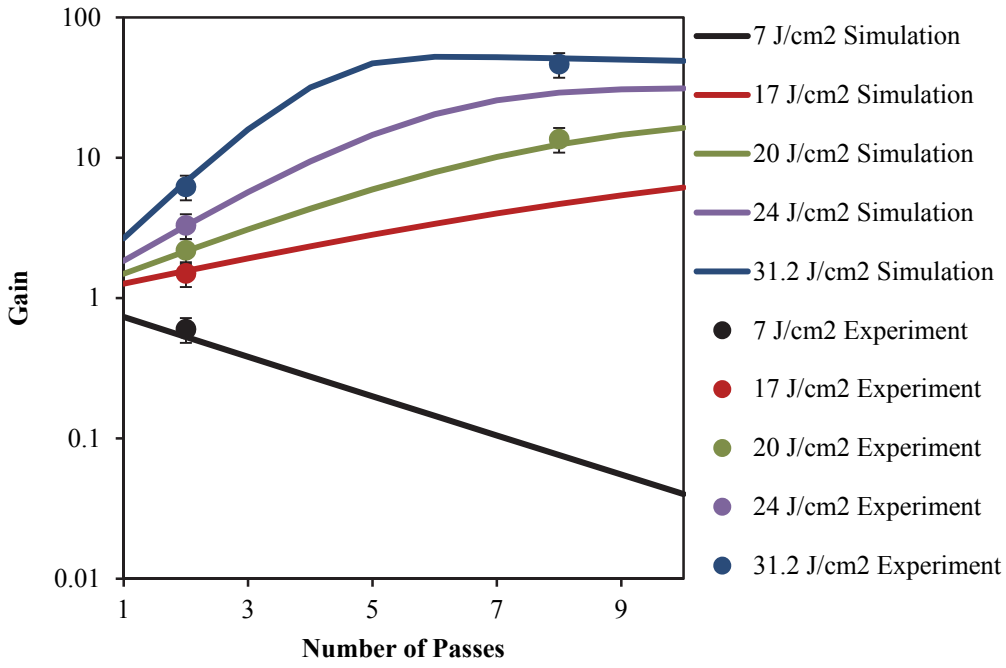

Figure 5.10: Comparison between the peak simulated and measured gain at different pump fluences with seed power of 127 W/cm^2, a seed beam diameter of 0.44 mm (FWHM) in the gain medium and 1ms pump pulse duration

5.5 Gain Measurement at Cryogenic Temperature

Once agreement was found with the room temperature measurements, the behavior of the Yb:YAG crystal at cryogenic temperatures was studied. To measure the gain at cryogenic temperatures the crystal was placed in the cryogenic chamber described previously. The photo diode output voltages after double pass through the gain medium at room temperature and at 250K are compared in figure 5.11. However, at very low temperature, very high gain also can lead to parasitic lasing. For an example, figure 5.12 shows a screen shot of the oscilloscope where the gate pulse used to drive the pump diode laser is measured in channel 1, the pump diode current is measured in channel 2, and the photo diode voltage used to measure the output power of the amplifier is shown in channel 3 where a 12 kΩ termination resistor was used. When the there is no pump, the photo diode measured the seed power after the losses form the optics and the crystal absorption. When the pump turns on, the signal starts to get amplified and the photo diode voltage keeps on increasing over time until the pump current is on as shown in figure 5.11. However, the figure 5.12 shows that the photodiode voltage increases for a small amount of time but starts to drop after 0.2 ms. This happens due to parasitic lasing in the crystal. In this example the pump current applied is 100 A (100 mV, Channel 2) which corresponds to a pump fluence of ~20 J/cm^2. At room temperature, we did not see anything like this behavior but at 86 K, we see this saturation effect. This is mainly because at lower temperature, the absorption around 1030 nm is reduced. Therefore, the threshold for parasitic transverse lasing is also reduced since there are deduced

passive losses in the beam path from the unpumped Yb:YAG media. As a result at lower temperature, the parasitic lasing killed the actual gain. Because of this we had to operate at an intermediate temperature to enhance the gain but avoid the parasitic lasing. Several measurements at different temperatures are shown in figure 5.13 where the gain keeps increasing with decreasing temperature until the parasitic lasing starts. The threshold gain for the parasitic lasing decreases with decreasing temperature because the absorption near 1030 nm decreases. The maximum double pass gain we have measured without noticeable parasitic lasing is 22.3 at 250 K. Another advantage of cooling the crystal is the absorption cross section around 1030 nm also decreases, which increases the effective gain of the amplifier. The double pass transmission factor measured at different temperatures is shown in figure 5.14. The measured gains seems to agree with our model calculation quite well as shown in figure 5.16. It is important to mention that in the simulation, the wavelength shift of the pump spectrum shown in figure 5.2 is considered by using the wavelength at the peak of the spectrum but the temporal drift in wavelength is not considered.

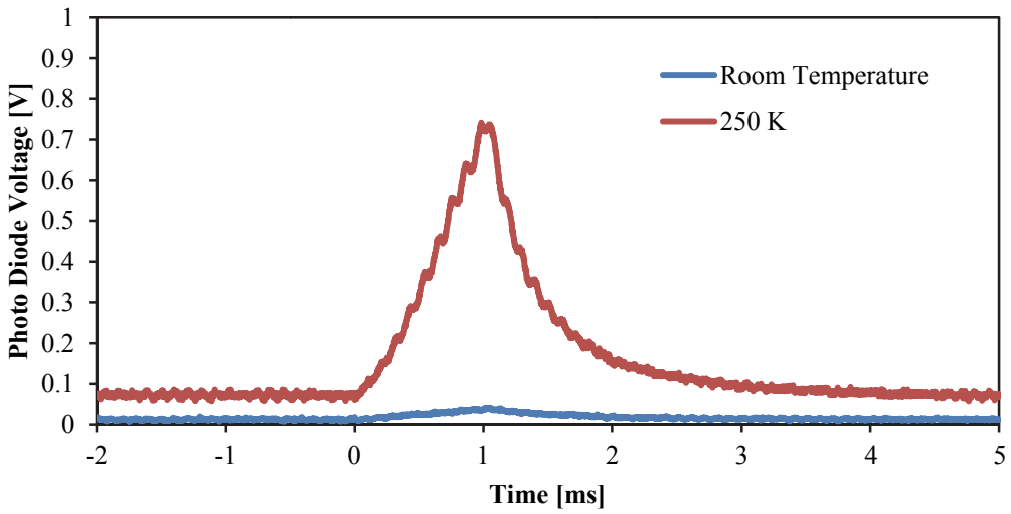

Figure 5.11: Comparison of the photodiode output voltage at 250 K with room temperature (pumped at 18 J/cm^2)

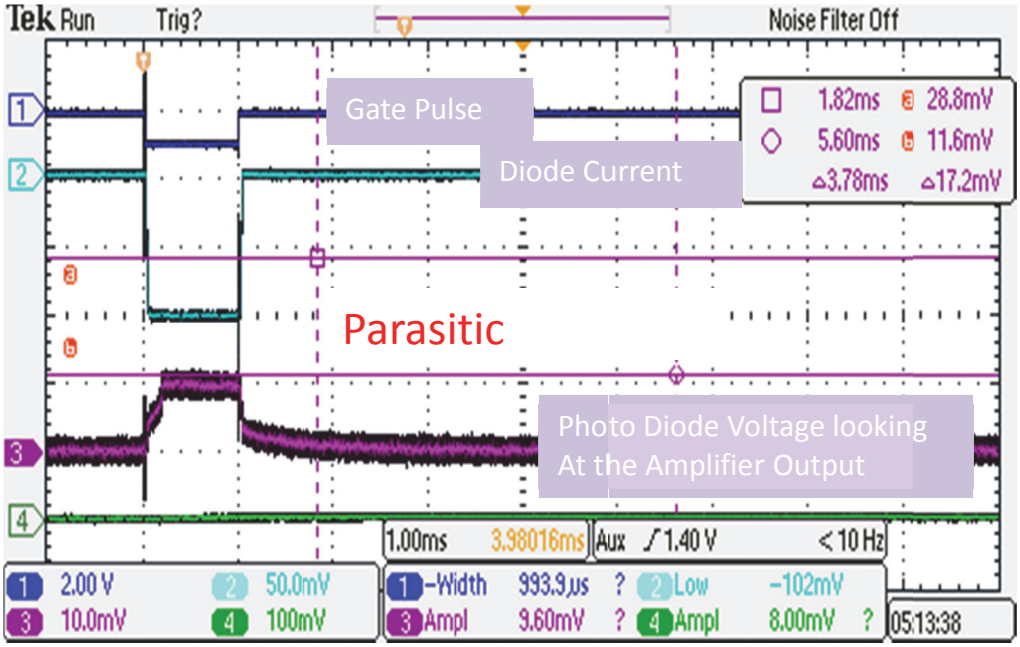

Figure 5.12: Oscilloscope traces of the gain measurements: The pump current is shown in channel 1, the pump power in channel 2 and the laser output power, as measured by a photodiode in channel 3. The photo diode voltage (channel 3) starts to saturate due to parasitic lasing at 86 K.

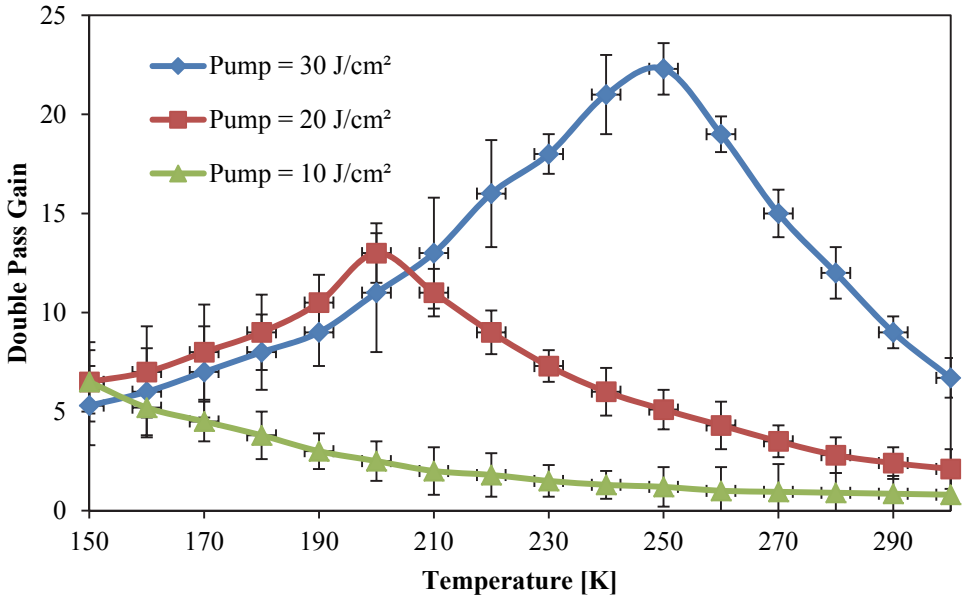

Figure 5.13: Measured double pass gain versus temperature for different pump fluences

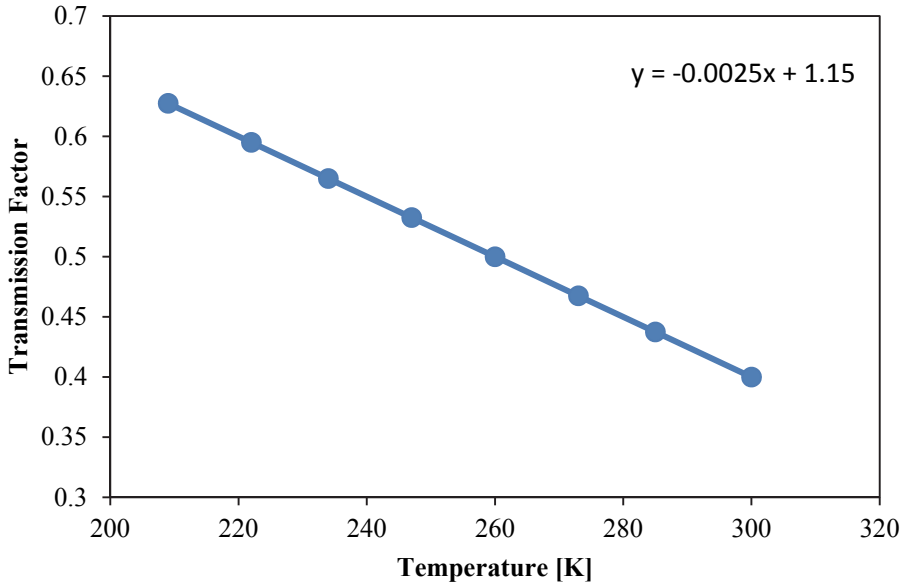

Figure 5.14: Double pass transmission factor of the crystal at 1030 nm

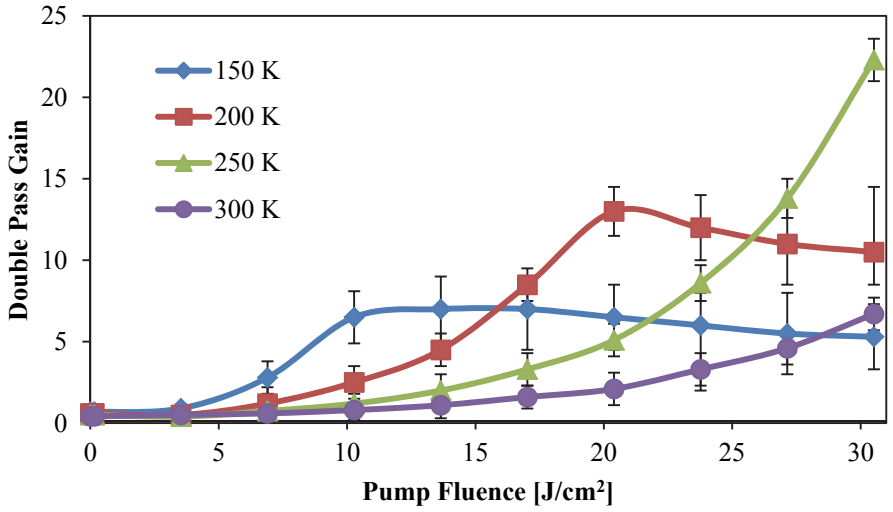

Figure 5.15: Double pass gain measured at difference temperature. Strong ASE/Parasitic lasing is observed below 250 K.

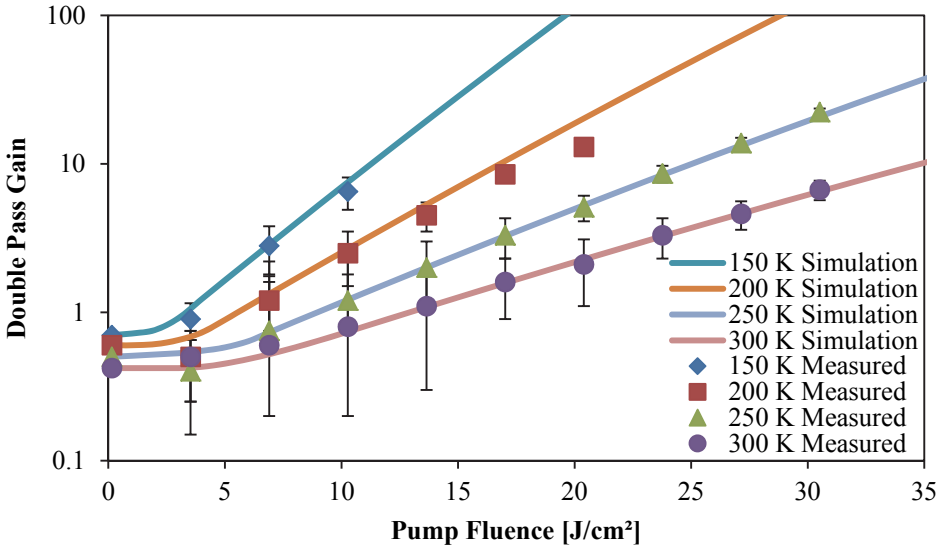

Figure 5.16: Comparison of simulation and experimental measurement with seed fluence of 1.27 mW/cm^2. The part of the datapoints affected by severe ASE/parasitic lasing are omitted

To achieve efficient energy extraction from laser amplifiers one requires final pass energy fluences on the order of F_{sat}. At room temperature with energy fluences of the order of $F_{sat} = 9.2$ J cm^{-2} this would be close to the damage threshold of the surfaces [6,73]. However, cooling to lower temperatures such as 250 K, would reduce $F_{sat}$to 5.7 that would allow higher gains per pass and efficient extraction while still remaining below the damage threshold. Cooling also reduces the thermal population in the lower laser level, changing the operation from a quasi-three level to a true four level laser system, which also improves the overall efficiency [74]. While the emission peak increases in magnitude with cooling, it decreases in width from ~8.3 nm (FWHM) at room temperature to ~5.5 nm at 250 K as shown in figure 5.17 [11]. For Gaussian pulse the minimum transform limited pulse width is given by the time bandwidth product $\Delta\nu\ \tau = 0.44$ for which a 10 nm bandwidth would lead to a pulse duration of ~150 fs, Spectral narrowing of the amplified pulse reduces the pulse bandwidth to a fraction of this value and final compressed pulse widths of the order picoseconds at 250 K could be expected.

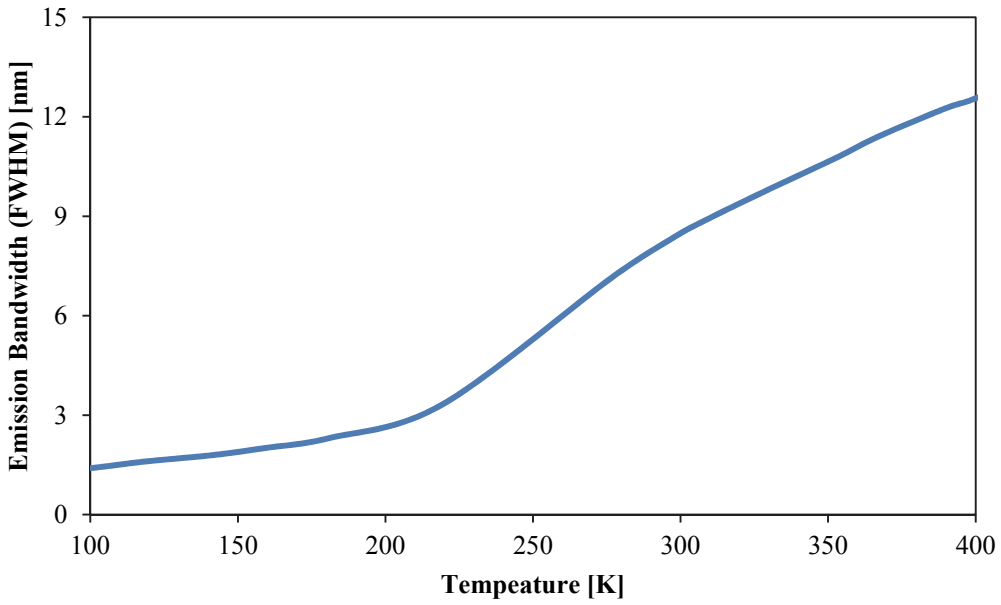

Figure 5.17: Emission bandwidth of Yb:YAG vs. temperature [11]

5.6 Scaling the System to Produce Terawatt pulses

Since our measurements at 250 K agrees with our model calculation, we performed our calculation at this temperature to scale the system up to terawatt level. A conventional Chirped Pulse Amplification (CPA) requires a stretcher to reduce the original pulse intensity coming from a mode locked oscillator. Then the pulse should be amplified and then compressed back using a compressor. A 5 nJ pulse of duration 100 fs is a reasonable expected pulse from a mode-locked laser and an 80% efficient stretcher will reduce the pulse energy to 4 nJ. So we performed our calculation to design the system that will amplify a 4 nJ pulse to Joule level. Compressing a few Joule pulse to few picoseconds will give us a terawatt pulse. The amplifier we have developed can amplify a 0.5 mm seed beam of 4 nJ pulse energy to 16 mJ after 11 passes if we pump the a 10 at. % doped 2 mm Yb:YAG ceramic gain medium with 30 kJ/cm^2 fluence at 250 K as illustrated

in figure 5.18. The solid angle currently available in the cryogenic chamber will support up to a 4 double pass geometry but having a 5 double passes will require a longer focal length lens. Therefore, we have performed our next step assuming that the first stage will have a 4 double pass or 8 passes geometry. After 4 double passes, the output energy will reach to ~530 μJ.

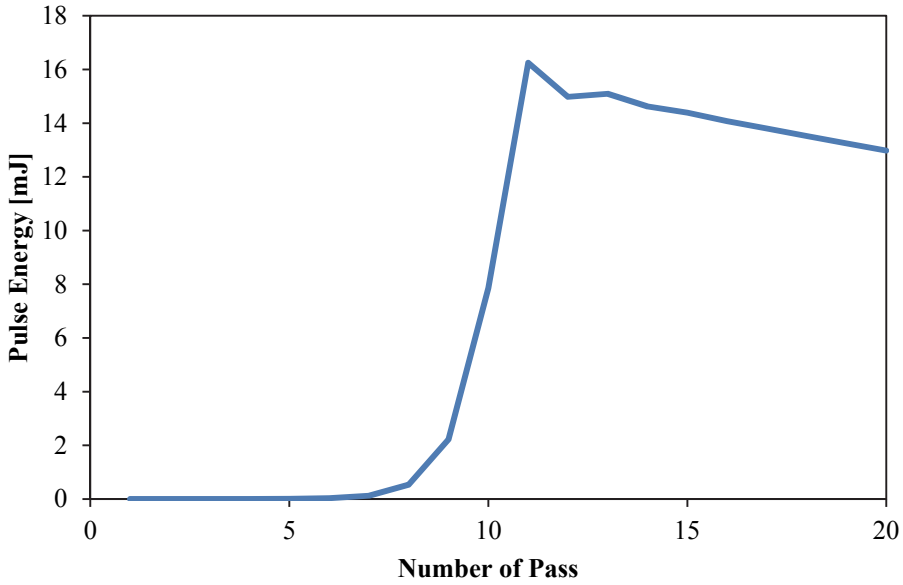

Figure 5.18: Evolution of pulse energy in the first stage amplifier after multiple passes for 30 J/cm^2 pump fluence at 250 K

With some mirror losses we assume a seed energy of 500 μJ as input of the second stage amplifier. To amplify the pulse to multi-joule level, we need to increase the diameter of the beam to at least 1.5 cm (FWHM). It means we need to pump a larger area of 1.5 × 1.5 cm^2. A seed beam of diameter 1.5 cm of 500 μJ pulse energy would require 6 passes to reach ~3.5 J as shown in figure 5.19. Having 8 passes will amplify the pulse to ~15 J but having 8 passes in a cryogenic chamber with 1.5 cm diameter might not be so easy. Therefore, for safe

approximation, we considered 6 passes for our calculation. Finally an 85% efficient grating compressor will give us an output of 3 J pulse.

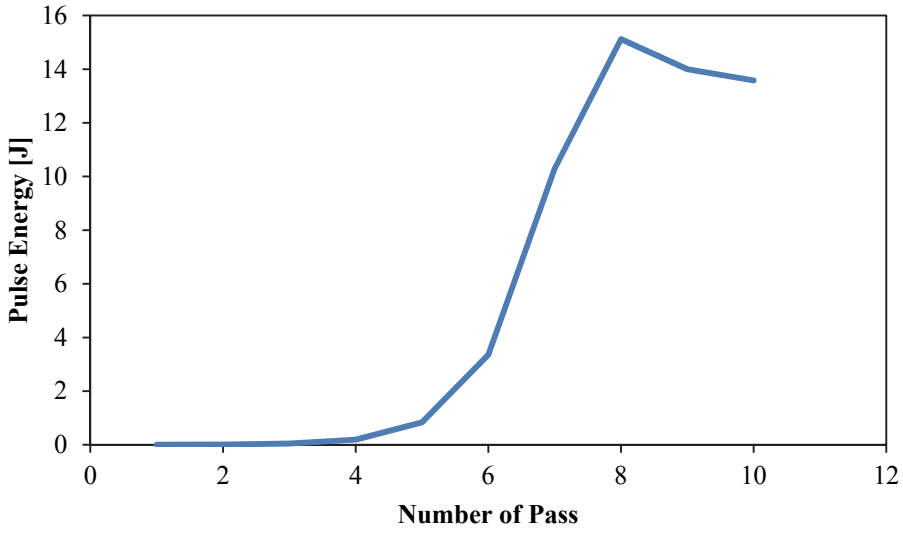

Figure 5.19: Evolution of pulse energy in the second stage amplifier after multiple passes for 30 J/cm^2 pump fluence at 250 K

We estimate that the gain narrowing effect of the high gain system will reduce the bandwidth of the signal to ~0.6 nm. The transform limited Gaussian pulse should allow us to compress the pulse to ~2.6 ps. If we expect a compressed pulse duration of 3 ps, then we get 1 TW output from the system.

5.7 Proposed Terawatt Laser Design

Considering all the aspects explained and the calculations performed in the previous section, we can propose a terawatt laser system as shown in figure 5.20. In this system, an oscillator generating 5 nJ pulse of duration 1 ps at 1030 nm wavelength is used as a seed source. The seed pulse is then stretched to 1000 ps in a grating stretcher with 80% efficiency reducing the pulse energy to 4 nJ. The

stretched pulse is then amplified in a 4 double pass 10 at. % doped Yb:YAG ceramic laser amplifier in active mirror configuration. The expected output from this amplifier is 530 µJ. With some mirror losses, 500 µJ pulse is again amplified in 3 double pass in a second stage cryogenic Yb:YAG amplifier. In this amplifier the pulse energy is amplified to 3.5 J. The pulse is then compressed to 3 ps using a grating compressor with 85% efficiency. The final output we can expect from this amplifier is therefore 3 J in 3 ps i.e. 1 TW pulse.

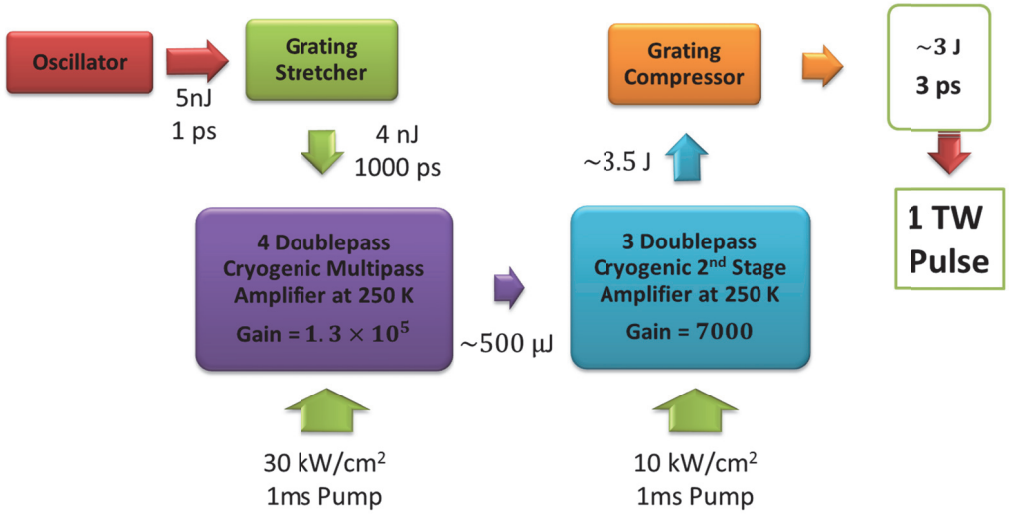

Figure 5.20: Proposed design of a terawatt system

The highest nanosecond scale pulse energy reported in a Yb:YAG system to date is 14 J at 2 Hz repetition rate of duration 8 ns by LULU group in France [15]. STFC Rutherford Appleton Laboratory has reported 7.4 J at 10 Hz and 9.4 J at 1 Hz [35]. The Colorado State university group in USA has reported pulse energy of 1 J at 10 Hz of pulse duration of 8.5 ps [3]. In 2014, Max-Planck-Institut für Quantenoptik group has also joined the joule class nanosecond output pulse lasers

by reporting a pulse energy of 0.8 J at 1 Hz with a pulse duration of 740 fs. Our proposed system would produce at least 3 J of pulse duration of 3 ps. Using a absorptive cladding layer on the edge of the laser medium would allow us to reach even higher gains and higher pulse energy. Since our pump pulse duration is 1 ms, in principle we could reach a repetition rate of 1 kHz but considering the cooling requirements to avoid thermal distortion of the beams and safe operation of the pump diodes we could expect to easily achieve 10 Hz repetition rate as other demonstrated systems to date.

5.8 Future Improvements

The main limitation of the system is the transverse lasing or parasitic lasing. We have observed the fluorescence power while blocking different mirrors or any reflective objects. In each case, we have seen the same parasitic lasing behavior. It confirms that the parasitic lasing is most likely happening due to the reflection from the edges of the gain medium. Although the edges of the gain medium are ground, at low temperature the absorption cross-section at 1030 nm wavelength of the unpumped region surrounding the pumped region is reduced so much and the peak gain increases so much that the parasitic lasing occurs even due the scattering from the edges. Currently we can avoid this problem by adding heat to the crystal mount using two chasis mount resistors. Operating at an intermediate temperature allows us to work just below the parasitic lasing threshold. In this way we are getting enough gain from the crystal to develop a terawatt system but the gain can be increased much more if we could eliminate the reflection from the edges of the gain medium. Many groups have solved this problem by adding an

absorbing cladding layer around the gain medium. For an example, the LULI group [15] in Ecole Polytechnique in France has increased the Yb:YAG diameter significantly so that the unpumped region can work as a self cladding layer to absorb the fluorescence. However, currently they found that using a Cr^{4+}:YAG cladding layer around Yb^{3+}:YAG is better and can be done economically without major engineering. The STFC Rutherford Appleton Laboratory group [56] in UK has also used a 10 mm Cr^{4+}:YAG cladding layer around a 35 mm diameter Yb:YAG ceramic as an absorption layer. The HiLASE project group has proposed using of a Ni-Ta_2O_5 layer to reduce ASE/ parasitic lasing in 2011 [75] but finally decided to use a 30 mm thick Cr^{4+}:YAG layer around a $60 \times 60\ mm^2$ Yb:YAG crystal for their final design [76].

From the results of different groups working around the world, it seems like using the Cr^{4+}:YAG cladding layer around the Yb:YAG ceramic gain medium is the easiest and widely accepted solution to solve the problem of parasitic lasing. Thus we would propose that the final amplifier medium be ordered with such a cladding region which is fairly easy to do for ceramic based materials.

We can also consider replacing the first stage cryogenic amplifier with a room temperature regenerative amplifier to reduce the gain narrowing effect. A regenerative amplifier can support high number of passes to compensate the low gain per pass at room temperature. Therefore, we can get the required pulse energy with broader bandwidth after the first stage. This will allow shorter pulse durations.

A wide range of absorption and emission cross-sections are published in the literature. Cross-sections found in [10] have given us results very close to the measurements of our system. It does not mean that these values are the most appropriate values. It depends on the manufacturing process of the crystal and also the quality of the doping. The recent literature values range from $0.9 \times 10^{-20}\,\mathrm{cm}^2$ to $1 \times 10^{-20}\,\mathrm{cm}^2$ for the peak absorption cross-section and $2.1 \times 10^{-20}\,\mathrm{cm}^2$ to $2.4 \times 10^{-20}\,\mathrm{cm}^2$ for the peak emission cross-section. Therefore, measuring the absorption and emission cross-section of the amplifier crystal precisely would allow us to predict the performance more accurately.

For femtosecond operation we have to switch to a crystal such as Yb:CaF_2 or Yb:LuAG because they also offer higher gain at low temperature but the emission bandwidth is significantly broader at lower temperature [10]. However, since their emission cross-sections are significantly lower than Yb:YAG, a regenerative amplifier would probably be required to extract enough stored energy.

Chapter 6 Conclusion

A Yb:YAG ceramic multipass laser amplifier has been developed and characterized at room temperature and cryogenic temperatures. A maximum double pass gain of 6.5 is measured at room temperature with 30 J/cm^2 of pump fluence. No significant ASE or transverse lasing are observed at room temperature. However, ASE spectrum narrowing is observed with the pump intensity indicating significant ASE amplification.

A cryogenic vacuum chamber was developed for low temperature operation of the amplifier. Use of liquid nitrogen allows the temperature of the crystal to be cooled down to 77 K. Although a significant increase in gain is observed at lower temperatures, we could not operate with high pump fluences below 250 K due to parasitic lasing. At 250 K a peak small signal double pass gain of 22.3 was measured at a pump fluence of 30 J/cm^2. The variation of gain with the pump intensity and temperature was characterized.

A 2D model in Matlab for quick calculations and a 3D model in Comsol for precision calculation has also been developed. With suitable choice of gain and absorption coefficients, the model calculations agree quite well with the measurements as long as significant parasitic lasing does not extract significant of stored energy since ASE was not considered in our model. This agreement gives us confidence that the modeling code can be used for designing a high energy amplifier system.

Based on the measurement and the model calculations, a terawatt system design has been proposed for future work. Our double pass gain measurement show that we have enough gain in the system that a combination of two such amplifier stages should be capable of producing few picosecond pulses of the joule level. It is also proposed that a two stage amplifier system at slightly cryogenic temperatures is sufficient to produce terawatt pulses. This would be equivalent to a number of high intensity Yb:YAG laser system groups around the world but with simple architecture not requiring a regenerative amplifier. Large gain can be achieved in the first stage by multiple passes through the amplifier region with very small beam diameters.

Due to the spectral narrowing of emission cross-section at lower temperatures, pulse widths below a few picoseconds would require some spectral compensation techniques to broaden the gain peak. The gain can also be further increased by quenching the parasitic lasing. One solution could be to use an absorbing Cr^{4+}: YAG cladding layer around the Yb:YAG ceramic gain medium. This layer will would absorb 1030 nm and light and hence will reduce the backscatter feedback suppressing parasitic lasing.

The present work has characterized Yb:YAG ceramic laser media at cryogenic temperatures and developed effective modeling codes to allow for scaling to Terawatt class laser system. Overall, the results look promising to allow for scaling to efficient diode pumped terawatt lasers for future applications.

Bibliography

1. Yessik MJ. Laser Material Processing. *Optical Engineering*. 17(3), 173202–173202 (1978).

2. Ledingham K, McKenna P, Singhal R. Applications for nuclear phenomena generated by ultra-intense lasers. *Science*. 300(5622), 1107–1111 (2003).

3. Furch FJ, Reagan BA, Luther BM, Curtis AH, Meehan SP, Rocca JJ. Demonstration of an all-diode-pumped soft x-ray laser. *Optics letters*. 34(21), 3352–3354 (2009).

4. Strickland D, Mourou G. Compression of amplified chirped optical pulses. *Optics communications*. 55(6), 447–449 (1985).

5. Thales. Alpha XS 1 PW Ultrafast Ti:Sa Series Datasheet [Internet]. Available from: https://www.thalesgroup.com/sites/default/files/asset/document/alpha_pw_2014_0.pdf.

6. Do BT, Smith AV. Bulk optical damage thresholds for doped and undoped, crystalline and ceramic yttrium aluminum garnet. *Applied optics*. 48(18), 3509–3514 (2009).

7. Dong J, Bass M, Mao Y, Deng P, Gan F. Dependence of the Yb^{3+} emission cross section and lifetime on temperature and concentration in yttrium aluminum garnet. *JOSA B*. 20(9), 1975–1979 (2003).

8. Lacovara P, Choi H, Wang C, Aggarwal R, Fan T. Room-temperature diode-pumped Yb: YAG laser. *Optics letters*. 16(14), 1089–1091 (1991).

9. Ostermeyer M, Straesser A. Theoretical investigation of feasibility of Yb: YAG as laser material for nanosecond pulse emission with large energies in the Joule range. *Optics communications*. 274(2), 422–428 (2007).

10. Jambunathan V, Koerner J, Sikociniski P, *et al.* Spectroscopic characterization of various Yb^{3+} doped laser materials at cryogenic temperatures for the development of high energy class diode pumped solid state lasers. In: *SPIE Optics+ Optoelectronics*., 87800G–87800G (2013).

11. Körner J, Jambunathan V, Hein J, *et al.* Spectroscopic characterization of Yb3+-doped laser materials at cryogenic temperatures. *Applied Physics B*., 1–7 (2013).

12. Tümmler J, Jung R, Stiel H, Nickles P, Sandner W. High-repetition-rate chirped-pulse-amplification thin-disk laser system with joule-level pulse energy. *Optics letters*. 34(9), 1378–1380 (2009).
13. Tokita S, Divoky M, Furuse H, *et al.* Generation of 500-mJ nanosecond pulses from a diode-pumped Yb: YAG TRAM laser amplifier. *Optical Materials Express*. 4(10), 2122–2126 (2014).

14. Tokita S, Kawanaka J, Izawa Y, Fujita M, Kawashima T. 23.7-W picosecond cryogenic-Yb: YAG multipass amplifier. *Optics Express*. 15(7), 3955–3961 (2007).

15. Gonçalvès-Novo T, Albach D, Vincent B, Arzakantsyan M, Chanteloup J-C. 14 J/2 Hz Yb^{3+}: YAG diode pumped solid state laser chain. *Optics express*. 21(1), 855–866 (2013).

16. Saraceno CJ, Emaury F, Schriber C, *et al.* Toward millijoule-level high-power ultrafast thin-disk oscillators. (2015).

17. Tabak M, Hammer J, Glinsky ME, *et al.* Ignition and high gain with ultrapowerful lasers. *Physics of Plasmas (1994-present)*. 1(5), 1626–1634 (1994).

18. Dubietis A, Butkus R, Piskarskas AP. Trends in chirped pulse optical parametric amplification. *Selected Topics in Quantum Electronics, IEEE Journal of*. 12(2), 163–172 (2006).

19. Keller U. Recent developments in compact ultrafast lasers. *Nature*. 424(6950), 831–838 (2003).

20. DeMaria A, Stetser D, Heynau H. SELF MODE-LOCKING OF LASERS WITH SATURABLE ABSORBERS. *Applied Physics Letters*. 8(7), 174–176 (1966).

21. Maiman TH. Stimulated optical radiation in ruby. (1960).

22. Kuizenga DJ, Siegman A. FM and AM mode locking of the homogeneous laser-Part I: Theory. *Quantum Electronics, IEEE Journal of*. 6(11), 694–708 (1970).

23. Haus H. Theory of mode locking with a slow saturable absorber. *Quantum Electronics, IEEE Journal of*. 11(9), 736–746 (1975).

24. Haus H, Shank C, Ippen E. Shape of passively mode-locked laser pulses. *Optics Communications*. 15(1), 29–31 (1975).

25. Moulton PF. Spectroscopic and laser characteristics of Ti:Al_2O_3. *JOSA B*. 3(1), 125–133 (1986).

26. Hall R, Fenner G, Kingsley J, Soltys T, Carlson R. Coherent Light Emission from Ga-As Junctions. *Phys. Rev. Lett*. 9, 366 (1962).

27. Nathan MI, Dumke WP, Burns G, Dill Jr FH, Lasher G. Stimulated emission of radiation from GaAs p-n junctions. *Applied Physics Letters*. 1(3), 62–64 (1962).

28. Siebold M, Klingebiel S, Wandt C, *et al.* Diode-pumped ytterbium-based chirped-pulse amplifier. In: *XVII International Symposium on Gas Flow and Chemical Lasers and High Power Lasers*., 713110–713110 (2008).

29. Körner J, Hein J, Kahle M, *et al.* Temperature dependent measurement of absorption and emission cross sections for various Yb^{3+} doped laser materials. In: *SPIE Optics+ Optoelectronics*., 808003–808003 (2011).

30. Ben-Xue J, Tong-De H, Yu-Song W, *et al.* Comparative spectroscopic investigation of Yb-doped YAG, YSAG and YLaO3 transparent ceramics. *Chinese Physics B*. 17(9), 3407 (2008).

31. Pug\vzlys A, Andriukaitis G, Sidorov D, *et al.* Spectroscopy and lasing of cryogenically cooled Yb, Na: CaF2. *Applied Physics B*. 97(2), 339–350 (2009).

32. Koerner J, Hein J, Liebetrau H, *et al.* Temperature resolved measurements of absorption and emission cross sections for various Yb^{3+}-doped gain media from 100K to room temperature. In: *Lasers and Electro-Optics Europe (CLEO EUROPE/EQEC), 2011 Conference on and 12th European Quantum Electronics Conference*., 1–1 (2011).

33. Bayramian A, Armstrong P, Ault E, *et al.* The Mercury Project: A high average power, gas-cooled laser for inertial fusion energy development. *Fusion Science and Technology*. 52(3), 383–387 (2007).

34. Hornung M, Keppler S, Bödefeld R, *et al.* High-intensity, high-contrast laser pulses generated from the fully diode-pumped Yb: glass laser system POLARIS. *Optics letters*. 38(5), 718–720 (2013).

35. Ertel K, Banerjee S, Mason PD, *et al.* DiPOLE: a scalable laser architecture for pumping multi-Hz PW systems. In: *SPIE Optics+ Optoelectronics*., 87801W–87801W (2013).

36. Siebold M, Roeser F, Loeser M, Albach D, Schramm U. PEnELOPE: a high peak-power diode-pumped laser system for laser-plasma experiments. In: *SPIE Optics+ Optoelectronics*., 878005–878005 (2013).

37. Curtis A, Reagan B, Wernsing K, Furch F, Luther B, Rocca J. Demonstration of a compact 100 Hz, 0.1 J, diode-pumped picosecond laser. *Optics letters*. 36(11), 2164–2166 (2011).

38. Ogawa K, Akahane Y, Yamakawa K. 100-mJ diode-pumped, cryogenically-cooled Yb: YLF chirped-pulse regenerative amplifier. In: *CLEO: Science and Innovations*., CMB4 (2011).

39. Metzger T, Teisset CY, Krausz F. High-repetition-rate picosecond pump laser based on a Yb: YAG disk amplifier for optical parametric amplification. In: *Advanced Solid-State Photonics*., TuA2 (2008).

40. Papadopoulos DN, Pellegrina A, Ramirez LP, Georges P, Druon F. Broadband high-energy diode-pumped Yb: KYW multipass amplifier. *Optics letters*. 36(19), 3816–3818 (2011).

41. Ogawa K, Akahane Y, Aoyama M, *et al.* Multi-millijoule, diode-pumped, cryogenically-cooled Yb: $KY(WO_4)_2$ chirped-pulse regenerative amplifier. *Optics express*. 15(14), 8598–8602 (2007).

42. Akahane Y, Aoyama M, Ogawa K, *et al.* High-energy, diode-pumped, picosecond Yb: YAG chirped-pulse regenerative amplifier for pumping optical parametric chirped-pulse amplification. *Optics letters*. 32(13), 1899–1901 (2007).

43. Wandt C, Klingebiel S, Keppler S, *et al.* Development of a Joule-class Yb: YAG amplifier and its implementation in a CPA system generating 1 TW pulses. Laser & Photonics Reviews. (2014).

44. Einstein A. Zur quantentheorie der strahlung. *Physikalische Zeitschrift*. 18, 121–128 (1917).

45. Frantz LM, Nodvik JS. Theory of pulse propagation in a laser amplifier. *Journal of Applied Physics*. 34(8), 2346–2349 (1963).

46. Le Garrec B, Cardinali V, Bourdet G. Thermo-optical measurements of ytterbium doped ceramics (Sc_2O_3, Y_20_3, Lu_20_3, YAG) and crystals (YAG, CaF_2) at cryogenic temperatures. In: *SPIE Optics+ Optoelectronics*., 87800E–87800E (2013).

47. Fan TY, Ripin DJ, Aggarwal RL, *et al.* Cryogenic Yb^{3+}-Doped Solid-State Lasers. *Selected Topics in Quantum Electronics, IEEE Journal of*. 13(3), 448–459 (2007).

48. Bödefeld R, Koerner J, Siebold M, *et al.* Comparative damage study on ytterbium-doped materials for diode-pumped high energy lasers. In: *Boulder Damage Symposium XL Annual Symposium on Optical Materials for High Power Lasers*., 713214–713214 (2008).

49. Matsushima I, Tanabashi A. Development of high-efficiency 10 kHzmJps Yb: YAG laser for industry. *Optical review*. 17(3), 294–299 (2010).

50. Siebold M, Wandt C, Klingebiel S, *et al.* High-energy diode-pumped Yb: YAG chirped pulse amplifier. In: *Photonics Europe*., 69980E–69980E (2008).

51. Wang J, Zhang Z, Cheng X, *et al.* Study of diode-pumped Yb: YAG disk lasers at low temperature. *Chinese optics letters*. 9(11), 111403 (2011).

52. Lu X, Wang J, Jiang Y, Fan W, Li X. Transient thermal effects in end-pumped cryogenic Yb: YAG regenerative amplifier. *Journal of Modern Optics*. 59(4), 354–359 (2012).

53. Fu X, Hong K-H, Chen L-J, Kärtner FX. Performance scaling of high-power picosecond cryogenically cooled rod-type Yb: YAG multipass amplification. *JOSA B*. 30(11), 2798–2809 (2013).

54. Siebold M, Loeser M, Schramm U, *et al.* High-efficiency, room-temperature nanosecond Yb: YAG laser. *Optics Express*. 17(22), 19887–19893 (2009).

55. Banerjee S, Ertel K, Mason P, Hernandez-Gomez C, Collier J. Concept for Cryogenic kJ-Class Yb: YAG Pump Laser. In: *AIP Conference Proceedings*., 223 (2010).

56. Mason PD, Ertel K, Banerjee S, Phillips PJ, Hernandez-Gomez C, Collier JL. Optimised design for a 1 kJ diode-pumped solid-state laser system. In: *SPIE Optics+ Optoelectronics*., 80801X–80801X (2011).

57. Ertel K, Banerjee S, Mason P, *et al.* Optimising the efficiency of pulsed diode pumped Yb: YAG laser amplifiers for ns pulse generation. *Optics Express*. 19(27), 26610–26626 (2011).

58. Mason PD, Banerjee S, Ertel K, Phillips PJ, Greenhalgh J, Collier JL. DiPOLE-An Efficient and Scalable High Pulse Energy and High Average Power Cryogenic Gas Cooled Multi-Slab Amplifier Concept. *Plasma and Fusion Researh:Regular Articles*. 8, 3404051–1–4 (2013).

59. Banerjee S, Ertel K, Mason P, Phillips J, Greenhalgh J, Collier J. DiPOLE: A multi-slab cryogenic diode pumped Yb: YAG amplifier. In: *SPIE Optics+ Optoelectronics*., 878006–878006 (2013).

60. Banerjee S, Ertel K, Mason PD, *et al.* High-efficiency 10 J diode pumped cryogenic gas cooled Yb: YAG multislab amplifier. *Optics Letters*. 37(12), 2175–2177 (2012).

61. Lu X, Wang J, Li X, Jiang Y, Fan W, Li X. Theoretical and experimental research on cryogenic Yb: YAG regenerative amplifier. *Chinese optics letters*. 9(11), 111401 (2011).

62. Brown DC, Cone RL, Sun Y, Equall RW. Yb: YAG absorption at ambient and cryogenic temperatures. *Selected Topics in Quantum Electronics, IEEE Journal of*. 11(3), 604–612 (2005).

63. Ashoori V, Shayganmanesh M, Radmard S. Heat Generation and Removal in Solid State Lasers. (2012).

64. Farrukh UO, Buoncristiani AM, Byvik CE. An analysis of the temperature distribution in finite solid-state laser rods. *IEEE journal of quantum electronics*. 24, 2253–2263 (1988).

65. Diels J-C, Rudolph W. Ultrashort laser pulse phenomena. Academic press.

66. Aggarwal R, Ripin D, Ochoa J, Fan T. Measurement of thermo-optic properties of Y3Al5O12, Lu3Al5O12, YAIO3, LiYF4, LiLuF4, BaY2F8, KGd (WO4) 2, and KY (WO4) 2 laser crystals in the 80-300K temperature range. *Journal of Applied Physics*. 98(10), 103514 (2005).

67. Perry DL. Handbook of inorganic compounds. CRC press, (2011).

68. Taira T, Tulloch WM, Byer RL. Modeling of quasi-three-level lasers and operation of cw Yb: YAG lasers. *Applied optics*. 36(9), 1867–1874 (1997).

69. Smith AV, Do BT. Bulk and surface laser damage of silica by picosecond and nanosecond pulses at 1064 nm. *Applied optics*. 47(26), 4812–4832 (2008).

70. Reagan BA, Curtis AH, Wernsing KA, Furch FJ, Luther BM, Rocca JJ. Development of high energy diode-pumped thick-disk Yb: YAG chirped-pulse-amplification lasers. *Quantum Electronics, IEEE Journal of*. 48(6), 827–835 (2012).

71. Kissel H, Fassbender W, Lotz J, *et al.* Reliable QCW diode laser arrays for operation with high duty cycles. In: *SPIE LASE*., 86050V–86050V (2013).

72. Grossman WM, Olson TE, Plaessmann H. Multi-pass light amplifier. (1996).

73. Zelmon DE, Schepler KL, Guha S, *et al.* Optical properties of Nd-doped ceramic yttrium aluminum garnet. In: *Boulder Damage Symposium XXXVI*., 255–264 (2005).

74. Ikesue A, Aung YL. Ceramic laser materials. *Nature photonics*. 2(12), 721–727 (2008).

75. Sawicka M, Divoky M, Novak J, Mocek T, Rus B. Numerical evaluation of heat deposition in cryogenically cooled multi-slab amplifier. In: *SPIE Optics+ Optoelectronics*., 80800C–80800C (2011).

76. Sawicka M, Divoky M, Novak J, Lucianetti A, Rus B, Mocek T. Modeling of amplified spontaneous emission, heat deposition, and energy extraction in cryogenically cooled multislab Yb^{3+}: YAG laser amplifier for the HiLASE Project. *JOSA B*. 29(6), 1270–1276 (2012).